A new contribution to the Late Quaternary tephrostratigraphy of the Mediterranean: Aegean Sea core LC21

C. Satow [a, *], E.L. Tomlinson [b], K.M. Grant [c], P.G. Albert [d, e], V.C. Smith [d], C.J. Manning [e], L. Ottolini [f], S. Wulf [g], E.J. Rohling [c, h], J.J. Lowe [a], S.P.E. Blockley [a], M.A. Menzies [e]

[a] Department of Geography, Queens Building, Royal Holloway University of London, TW20 OEX, UK
[b] Department of Geology, Trinity College Dublin, Dublin 2, Ireland
[c] Research School of Earth Sciences, The Australian National University, Canberra, ACT, 0200, Australia
[d] Research Laboratory for Archaeology and the History of Art, University of Oxford, Dyson Perrins Building, South Parks Road, Oxford, OX1 3QY, UK
[e] Department of Earth Sciences, Queens Building, Royal Holloway University of London, TW20 OEX, UK
[f] Consiglio Nazionale Delle Ricerche, Istituto di Geoscienze e Georisorse (IGG) — Unità di Pavia, Italy
[g] Helmholtz Centre Potsdam, GFZ German Research Centre for Geosciences, Section 5.2, Telegrafenberg, D-14473, Potsdam, Germany
[h] Ocean and Earth Science, University of Southampton, National Oceanography Centre, Southampton, SO14 3ZH, UK

ARTICLE INFO

ABSTRACT

Tephra layers preserved in marine sediments can contribute to the reconstruction of volcanic histories and potentially act as stratigraphic isochrons to link together environmental records. Recent developments in the detection of volcanic ash (tephra) at levels where none is macroscopically visible (so-called 'crypto-tephra') have greatly enhanced the potential of tephrostratigraphy for synchronising environmental and archaeological records by expanding the areas over which tephras are found. In this paper, crypto-tephra extraction techniques allow the recovery of 8 non-visible tephra layers to add to the 9 visible layers in a marine sediment core (LC21) from the SE Aegean Sea to form the longest, single core record of volcanic activity in the Aegean Sea. Using a novel, shard-specific methodology, sources of the tephra shards are identified on the basis of their major and trace element single-shard geochemistry, by comparison with geochemical data from proximal Mediterranean volcanic stratigraphies. The results indicate that the tephra layers are derived from 14 or 15 separate eruptions in the last ca 161 ka BP: 9 from Santorini; 2 or 3 from Kos, Yali, or Nisyros; 2 from the Campanian province; and one from Pantelleria. The attributions of these tephra layers indicate that 1) inter-Plinian eruptions from Santorini may have produced regionally significant tephra deposits, 2) marine tephrostratigraphies can provide unique and invaluable data to eruptive histories for island volcanoes, and 3) tephra from both Pantelleria and Campania may be used to correlate marine records from the Aegean Sea to those from the Tyrrhenian, Adriatic and Ionian Seas.

1. Introduction

Volcanic eruptions inject ash (tephra) into the atmosphere, where it is widely distributed by winds. In particular Plinian and ultra-Plinian eruptions eject ash clouds into the stratosphere, where strong stratospheric winds can transport the tephra thousands of kilometres away from its source. The tephra falls out of the air and becomes preserved within depositional environments. The most explosive eruptions can distribute tephra over areas of 100,000 km^2 (e.g., Eastwood and Pearce, 1998; Wulf et al., 2002; Pyle et al., 2006; Margari et al., 2007; Aksu et al., 2008), providing potentially widespread markers for high precision correlations between a wide range of environmental and archaeological contexts (tephrostratigraphy). Consequently, tephra layers can provide excellent stratigraphic links between the various archives, with sufficient precision to address questions of the relative timings of events in archaeological or climate proxy data from those same archives, even at the sub-centennial scale (e.g. Lane et al., 2011; Lowe et al., 2012). In addition, if a tephra layer can be precisely dated, either from proximal deposits or a well-constrained

* Corresponding author. Current address: Dept. Geography, Kingston University, Kingston Upon Thames, Surrey, KT1 2EE, UK. Tel.: +44 02084 172 950.
E-mail address: c.satow@kingston.ac.uk (C. Satow).

distal record, then this single date can be imported into all records where that tephra layer is found (Lowe et al., 2012; Bronk Ramsey et al., 2014). The identification of a particular tephra layer relies on assessment of its stratigraphic position with respect to other tephras and, crucially, on precise determination of the tephra geochemistry. The geochemistry informs initially on the volcanic source of the tephra layer (Clift and Blusztajn, 1999), and subsequently, if a comprehensive reference database exists for potential sources, links to an individual eruption may be resolved. Tephra investigations have become more common in the past decade or so, as techniques to characterise the geochemistry of glass shards have improved (e.g., Pearce et al., 2004; Tomlinson et al., 2010).

Tephra layers preserved in marine sediments can contribute to the reconstruction of volcanic eruption histories and potentially act as stratigraphic isochrons to link together environmental records. In the late Quaternary abyssal sediments of the eastern Mediterranean, which is the focus of the present paper, this has long been realised through pioneering studies by.

for example, Richardson et al. (1976), Cita et al. (1977), Keller (1978), Federman and Carey (1980), Sparks et al. (1983), and Vinci et al. (1984, 1985). These studies revealed that a number of distinctive tephra layers are widespread throughout the region, and are common to, and therefore link, deep marine sediment sequences. Other studies have focused on tracing some of the ash layers to source volcanoes, especially the more distinctive layers, such as the Minoan tephra and 'Campanian Tuff' (Campanian Ignimbrite) (e.g. Sparks et al., 1983; Cramp et al., 1989), or on establishing their precise ages by a variety of dating techniques, including the $^{40}Ar-^{39}Ar$ method (e.g. Smith et al., 1996). These works have laid the foundations for the evolution of a comprehensive tephra framework, which has gradually been refined as tephra investigations in the region have progressively proliferated (see e.g. Vezzoli, 1991; Narcisi et al., 1999; Zanchetta et al., 2011). The discovery of some of these layers in distal localities has also extended the reach of the tephra framework, such as finding (inter alia) the Cape Riva and Campanian Ignimbrite layers in cave sequences and peat deposits in Greece (e.g. Vitaliano et al., 1981; St. Seymour and Christanis, 1995; St. Seymour et a., 2004). Notable developments also include the discovery of Santorini Minoan tephra in western Turkey (Eastwood et al., 1998) and the first discovery of a tephra derived from Anatolia in eastern Mediterranean deep-sea sediments (Hamann et al., 2010).

These investigations to date have been limited to tephra that is visible to the naked eye (e.g., Eastwood et al., 1999; Wulf et al., 2002; St Seymour et al., 2004; Margari et al., 2007; Aksu et al., 2008). However, recent investigations of marine cores have shown that crypto-tephra processing of a sequence can substantially augment the number of tephras found (e.g. Bourne et al., 2010). Here we apply such techniques to marine sediment core LC21 from the SE Aegean Sea (Fig. 1).

2. Previous work on core LC21

Core LC21 has been a focus for palaeoceanographic research in the Eastern Mediterranean since it was collected in 1995 (e.g., Hayes et al., 1999; de Rijk et al., 1999; Rohling et al., 2002b, 2004; Casford et al., 2002, 2003; Marino et al., 2007, 2009; van der Meer et al., 2007; Abu-Zied et al., 2008; Osborne et al., 2010). Studies have in general focused on the Holocene Sapropel S1 and the Eemian Sapropel S5. S1 is amenable to ^{14}C dating while ages for S5 have been inferred by correlation to the Soreq Cave speleothem data (Rohling et al., 2002a; Bar-Matthews et al., 2000; Marino et al., 2007, 2009). Recent work has elaborated the LC21 chronology in a probabilistic manner, based on a physical process-based correlation of its surface-water foraminiferal $\delta^{18}O$ record to the nearby U/Th

dated Soreq Cave $\delta^{18}O$ record, throughout the last 160,000 years (Grant et al., 2012).

Previous studies on core LC21 do not include comprehensive tephra investigations in their chronological framework. Casford et al. (2002, 2007) present AMS ^{14}C dates, but marine radiocarbon dates are subject to considerable uncertainty (e.g. Ascough et al., 2005; Lowe et al., 2007). Rohling et al. (2002a) and Marino et al. (2007) conclude, from statistically assessed event stratigraphies through Last Interglacial sapropel S5 in several different eastern Mediterranean sites, that the development of anoxic bottom-waters conditions (an inducing condition for sapropel formation) was distinctly time transgressive, and that the Aegean Sea led ecological changes in the open eastern Mediterranean by 300 ± 120 years (Marino et al., 2007). Tephrostratigraphy has the potential to bring much tighter control on the synchronisation of records in such studies, and a robust framework of tephra layers as synchronous stratigraphic markers may thus enhance studies of process relationships in Mediterranean palaeoceanography (e.g. Siani et al., 2003; Paterne et al., 2008; Bourne et al., 2010; Albert et al., 2012, in press).

We present a detailed tephrostratigraphical record for southeastern Aegean marine sediment core LC21, with its recent chronological constraints (Grant et al., 2012). The results contribute to the tephrochronological framework for the eastern Mediterranean and potentially to the eruptive histories of its volcanoes.

3. Materials and methods

3.1. Sampling and sample processing

Core LC21 was recovered in 1995 by *RV Marion Dufresne* during the EC-MAST2 PALAEOFLUX sampling program, at 35°40′N, 26°35′E (Fig. 1), with a present-day water depth of 1522 m. The recovered sequence of LC21 consists of hemi-pelagic sediments, organic-rich sapropel layers and visible tephra layers (Fig. 2). The excellently preserved archive half of the core was sub-sampled using u-channels at the BOSCORF facility, National Oceanography Centre, Southampton. Fig. 2 shows the locations within the core of the tephra samples presented in this paper. Sampling the core using carefully inter-calibrated sets of parallel u-channels enabled the recovery of strictly co-registered samples for tephra (Fig. 2) and stable isotope analyses (Grant et al., 2012).

The visible tephra layers were sampled initially, with the bottom 1 cm (representing the first deposit recorded in the core) being used for geochemistry. The entire length of core LC21 was then contiguously sampled and processed for crypto-tephra (excluding visible tephra layers) with continuous 5 cm resolution samples which were dried and then weighed. The 5 cm samples from the organic-rich layers (sapropels) were heated in a furnace for 3.5 h at 550 °C. Non-organic samples were not ashed. All samples were soaked in 10% HCL for 30 min to dissolve carbonates. The residues were then sieved over 125 and 25 μm meshes to remove large detritus and clays. Each was then floated in a centrifuge, first at 1.95 kg/l and then at 2.55 kg/l using diluted sodium polytungstate to separate the volcanic glass shards from organic and mineral matter. The floated material was mounted onto a slide using Euparal and examined for crypto-tephra shards under a high-power (×200 or ×400) microscope. Counts of the shards were normalised to the mass of the sample to give shards/g dry sediment. This approach assumes a uniform density of the dry sediment, whether it contains tephra or not. Where tephra was found, the u-channels were re-sampled at 1 cm resolution in order to define the peaks in shard concentrations and to extract shards for chemical analysis. Minor peaks of shards directly above or below visible tephra layers are likely
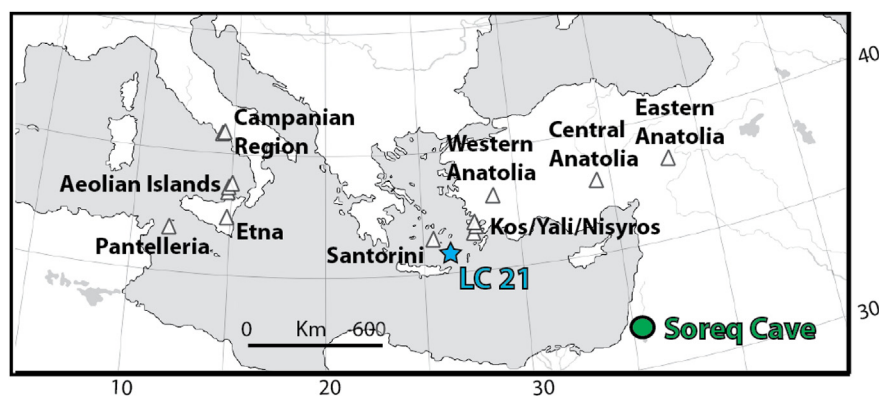
Fig. 1. Map showing the location of LC21, Soreq Cave and proximal volcanic sources considered in this paper. These are: Aeolian Islands (Lipari, Panaria, Salina, Stromboli, Vulcano), Anatolia (Western, Eastern and Central), Campanian Region (Ischia Island, Phlegrean Fields, Prochida, Vesuvius), Kos/Yali/Nisyros, Pantelleria, and Santorini.

to represent reworking by bioturbation and were not re-sampled (Watkins et al., 1978). Future studies could test this assumption using the methods of Cassidy et al. (2014). The re-sampling procedure was a replication of the 5 cm processing in all respects except, crucially, that none of the samples were ashed to remove organics, in order to preserve the chemical composition of the shards. Instead, a preliminary sodium polytungstate separation at 1.95 kg/l was used to remove organic matter as described by Blockley et al. (2005).

Extracted shards selected for chemical analysis were mounted onto pre-flattened resin stubs. Layers with either very low concentrations of tephra, or high concentrations of organic material remaining after processing, were mounted with the aid of a micro-manipulator and syringe to ensure exclusion of non-volcanic glass particles. The resulting sectioned and polished tephra shards were analysed for major and (where possible) trace element concentrations. A list of the samples analysed for geochemistry is provided in Table 1.

3.2. Electron probe micro-analysis (EPMA)

Analyses of 9 major elements (SiO_2, TiO_2, Al_2O_3, FeOt, MnO, MgO, CaO, Na_2O and K_2O) were performed at the Research Laboratory for Archaeology and the History of Art, University of Oxford, using a Jeol 8600 Electron Microprobe with 4 spectrometers with an accelerating voltage of 15 kV, beam diameter of 10 μm (defocused) and a low, 6 nA current (to minimise volatile loss). Count times were 30 s on each element peak except and Na_2O (10 s). Max Plank Institute (MPI-DING) standards StHs6/80 and ATHO-G (Jochum et al., 2007) were used to check the accuracy and precision of the EPMA analyses. Sodium was analysed first as it is known to be mobile during EPMA analyses (Hunt and Hill, 1993). Error bars on plots represent 2SD of replicate standard analyses run concurrently with the samples. Reproducibility is <10% relative standard deviation for analytes with concentrations >0.8 wt% with the exception of Na_2O (14—15%). Analytical data were filtered to remove analyses of non-vitreous material and those analyses with analytical totals lower than 90%. This value was used because water contents for rhyolitic glass shards can reach 9—10% (Pearce et al., 2008; Clift and Blusztajn, 1999; WoldeGabriel et al., 2005) and the volatiles and trace elements are not analysed using an electron microprobe. All analyses were normalised to 100% to account for volatile concentrations and secondary hydration (i.e. for comparative purposes). Accuracy is <5% at concentrations >0.8 wt% while analytes while accuracy for analytes <0.2 wt% can only be assessed qualitatively.

Each sample's stub surface was photographed prior to analysis to allow shards to be easily identified for analysis and to record the coordinates of each shard relative to 3 known points on the stub surface (the end of lines etched into the resin with a scalpel). A Cartesian co-ordinate transfer calculation enabled the same shards to be re-located for analysis on Laser Ablation Inductively Coupled Mass Spectrometry (LA-ICP-MS) or Secondary Ion Mass Spectrometry (SIMS). This procedure is vital when a tephra layer has a large geochemical range or multi-modal composition as the SiO_2 value for each shard is used as an internal standard for the trace element data. This shard-specific procedure allows different compositional modes to be detected.

3.3. Laser Ablation Inductively Coupled Plasma Mass Spectrometry (LA-ICP-MS)

Trace element analyses were obtained using an Aglient 7500 ce mass spectrometer coupled to a Resonetics 193 nm ArF excimer laser ablation system (RESOlution M−50 prototype) with a two-volume ablation cell (Muller et al., 2009) at Royal Holloway, University of London. Beam diameters of 25, 34 and 44 μm (appropriate to the size of the exposed shard surfaces) were used. The repetition rate was 5 Hz and the count time was 40 s (200 pulses) on the sample and 40 s on the gas blank (background). Concentrations were calibrated using NIST612 with [29]Si (from EPMA analysis) used as the internal standard. [43]Ca values of StHs6/80 were used for bias correction (Tomlinson et al., 2010). The same shards were analysed with the LA-ICP-MS system as were analysed with the EPMA. However, when the range of the shard SiO_2 values fell within the analytical precision of the EPMA additional shards were analysed on the LA-ICP-MS using the mean SiO_2 value for that sample to calibrate the trace element data (See Supplementary Information).

As with the EPMA results, the LA-ICP-MS data were filtered to only include glass data. By deleting parts of the shard analysis for which the elemental values indicate a mineral, void or resin component (Tomlinson et al., 2010) these components were removed from the final elemental values for each shard. Reproducibility of the ATHO-G and StHs 6/80-G (Jochum et al., 2007) analyses is typically <9% RSD for all trace elements. Accuracy is <5%.

3.4. Secondary Ion Mass Spectrometry (SIMS)

The secondary ion microprobe system at Consiglio Nazionale delle Ricerche Instituto di Geoscienze e Georisorse (CNR-IGG), Pavia, was used to obtain trace element data from samples with
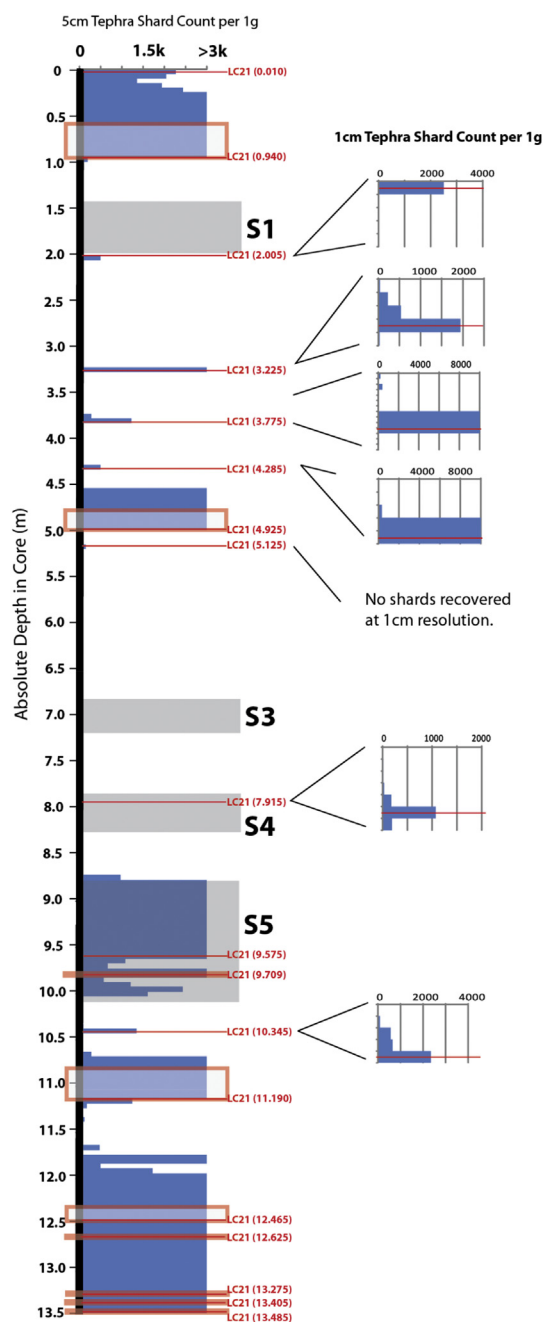
Fig. 2. The tephrostratigraphy of core LC21. 5 cm low resolution samples on left of diagram with tephra counts represented by blue bars (capped at counts >3000 shards per gram). Results of high resolution re-sampling at 1 cm resolution on the right of the diagram. Samples extracted and analysed for geochemistry are labelled with red lines and names, with the extent of visible tephras denoted by red boxes. The visual extents of sapropels (S1, S3, S4 and S5) are indicated by the grey areas and respective labels (e.g. S1). Core depth below the sea floor in meters is shown on the left of the diagram. (For interpretation of the references to colour in this figure legend, the reader is referred to the web version of this article.)

shards <25 μm in diameter. A $^{16}O^-$ beam (0.8–1.2 nA current) of between 5 and 8 μm was used, appropriate to the shard size. Experimental methods are similar to those adopted in Schiano et al. (2001, 2004), where the detailed SIMS procedure for REE (Rare Earth Element) de-convolution and quantification of ion signals for all trace elements is fully described. The width of the energy slit was 50 eV and the voltage offset applied to the accelerating voltage (+4500 V) was −100 V. Standards used for calibration interference

correction were NIST-SRM 610, BCR-2G (Le Roux et al., 2002), the intra CNR-IGG standard BB basalt glass and WY1 basaltic glass. Trace element concentrations were determined relative to the normalised (water free) SiO_2 EPMA data of the same shards. Accuracy is <4% for all analytes while reproducibility is <10% RSD.

4. Chronostratigraphic framework

The age model for the LC21 sequence has been constructed using the strong signal similarity between its high-resolution planktonic foraminiferal (*Globigerinoides ruber*) $\delta^{18}O$ record (Grant et al., 2012) and the extensively U/Th-dated Soreq Cave speleothem $\delta^{18}O$ record (Bar-Matthews et al., 2000, 2003) (Fig. 8). The strong signal similarity between these records reflects the fact that the eastern Mediterranean surface waters that bathe the site of LC21 are the source waters for precipitation over Israel (and thus the Soreq Cave catchment), with limited fractionation between the two areas, so that any isotopic changes in the eastern Mediterranean surface waters are reflected in the Soreq Cave record (so-called 'source-water effect'). This allows the radiometric chronology of the Soreq Cave record to be transferred to core LC21 (Grant et al., 2012), supplementing an array of AMS ^{14}C datings in the most recent 30,000 years. Two additional chronostratigraphic markers were provided by identification of the Minoan (Rohling et al., 2002b; Marino et al., 2009) and Campanian Ignimbrite (CI) (Lowe et al., 2012) tephra horizons in core LC21 (Fig. 8). The precision of the LC21 age model is further improved by the application of a Bayesian depositional model to the LC21 chronostratigraphy (Grant et al., 2012) using the OxCal software (Bronk Ramsey., 2008). The ages from the LC21 age model of Grant et al. (2012) are included here to provide age estimates for the tephra layers.

5. Results

The LC21 tephra layers are labelled by their depth in core in meters (between brackets), e.g., LC21 (4.925). The depth refers to the base of the sample selected for geochemistry. In visible layers, this is the base of the visible extent of the tephra. In crypto-tephra layers, this is the base of the sample that contains the peak in tephra concentrations (see summary in Table 1). The results of the 5 cm and 1 cm resolution tephra counts are presented in Fig. 2, alongside the sapropel stratigraphy, with the depths of the tephra samples taken for geochemical analysis. Large volumes of crypto-tephra are consistently found above visible tephra deposits. Such shard concentrations were interpreted as reworking by bio-turbation, as suggested by Watkins et al. (1978). Fig. 3 presents all the tephra shards analysed in this study on a total alkalis vs silica diagram. All geochemical data from LC21 are presented in Supplementary Figs. 1 and 2, and are provided as raw data in the Supplementary Information spreadsheet.

Sample LC21 (0.01) is the top 1 cm sample from LC21, which contained a shard concentration of 4808 shards/g. This peak in cryptotephra shard concentrations is above a 22.4 cm thick visible tephra layer (Fig. 2) and there are cryptotephra shards mixed into the sediment in the interval between the two. The shards show no evidence of chemical alteration but often contain micro-phenocrysts. The sample was geochemically characterised to assess its relationship to the visible tephra layer to ascertain if it consti-tuted a separate volcanic event or reworking of the visible tephra below (as suggested by Watkins et al., 1978). It is classified as rhyolitic with SiO_2 contents ranging from approximately 73.17 wt% to 74.27 wt% (Fig. 3). Total iron (FeOt) contents of the shards are 1.84–2.37 wt% while CaO contents are 1.26–1.5 wt%. Na_2O is greater than K_2O. 24 trace element analyses show that this sample has relatively low high field strength element (HFSE)

Table 1
Summary of major and trace element geochemistry for all tephra samples from LC21.

Tephra name in LC21	TAS classification (from Le Bas, 1986)	CaO/FeO	K₂O/Na₂O	Nb/Th	Zr/Th	Y/Th	La/Y	La/Nb
LC21 (0.01)	Rhyolite	0.68 ± 0.10	0.71 ± 0.06	0.80 ± 0.18	17.9 ± 1.3	2.20 ± 0.13	0.79 ± 0.05	2.21 ± 0.31
LC21 (0.94)	Rhyolite	0.68 ± 0.07	0.74 ± 0.06	0.71 ± 0.15	17.5 ± 1.4	2.19 ± 0.11	0.78 ± 0.04	2.47 ± 0.29
LC21 (2.005)	Rhyolite	0.68 ± 0.09	0.71 ± 0.07	0.72 ± 0.23	17.1 ± 1.6	2.14 ± 0.23	0.77 ± 0.04	2.39 ± 0.36
LC21 (3.225)	Rhyolite	0.69 ± 0.21	0.96 ± 0.97	0.66 ± 0.12	17.2 ± 1.5	2.26 ± 0.46	0.72 ± 0.05	2.47 ± 0.15
LC21 (3.775)	Trachydacite/Rhyolite	0.57 ± 0.33	0.65 ± 0.27	0.84 ± 0.05	19.7 ± 1.1	3.08 ± 0.17	0.63 ± 0.02	2.30 ± 0.06
LC21 (4.285)	Rhyolite	0.98 ± 0.19	0.96 ± 0.17	1.26 ± 0.12	11.8 ± 1.2	0.91 ± 0.15	1.99 ± 0.12	1.43 ± 0.09
LC21 (4.925)	Phonolite/Trachyte	0.63 ± 0.19	1.25 ± 0.60	2.60 ± 0.25	13.5 ± 0.6	1.10 ± 0.06	2.38 ± 0.03	1.01 ± 0.05
LC21 (5.125)	Rhyolite	0.67 ± 0.12	0.81 ± 0.54	0.68 ± 0.14	16.4 ± 1.2	1.84 ± 0.11	0.73 ± 0.02	2.05 ± 0.41
LC21 (7.915) Si-Saturated	Rhyolite	0.71 ± 0.22	0.73 ± 0.21	0.63 ± 0.11	16.6 ± 1.6	2.03 ± 0.17	0.79 ± 0.09	2.59 ± 0.34
LC21 (7.915) Si Undersaturated	Phonolite/Trachyte	0.67 ± 0.18	1.82 ± 1.86	3.14 ± 0.05	14.0 ± 0.3	1.13 ± 0.02	2.45 ± 0.07	0.88 ± 0.02
LC21 (9.575)	Andesite/Dacite/Trachydacite	0.66 ± 0.26	0.41 ± 0.17	1.18 ± 0.36	19.0 ± 2.5	4.64 ± 0.55	0.46 ± 0.06	1.96 ± 0.51
LC21 (9.709)	Dacite/Trachydacite	0.50 ± 0.05	0.66 ± 0.16	0.57 ± 0.02	16.3 ± 0.4	2.75 ± 0.07	0.52 ± 0.01	2.51 ± 0.07
LC21 (10.345)	Rhyolite	1.32 ± 1.84	1.58 ± 1.64	–	–	–	–	–
LC21 (10.345)	Pantellerite	0.04 ± 0.01	1.06 ± 1.10	–	–	–	–	–
LC21 (11.190)	Basaltic Andesite to Rhyolite	0.98 ± 0.90	0.47 ± 0.28	0.87 ± 0.28	18.1 ± 2.3	3.33 ± 0.85	0.56 ± 0.02	2.19 ± 0.17
LC21 (12.625)	Rhyolite	1.06 ± 0.17	1.27 ± 0.17	1.54 ± 0.07	3.3 ± 0.1	0.91 ± 0.04	1.63 ± 0.03	0.96 ± 0.02
LC21 (12.465)	Rhyolite	1.03 ± 0.24	1.27 ± 0.29	1.55 ± 0.08	3.3 ± 0.1	0.90 ± 0.03	1.65 ± 0.04	0.96 ± 0.04
LC21 (13.405)	Rhyolite	1.08 ± 0.33	1.27 ± 0.16	1.57 ± 0.13	3.3 ± 0.2	0.88 ± 0.03	1.70 ± 0.05	0.96 ± 0.03
LC21 (13.275)	Rhyolite	1.11 ± 0.34	1.30 ± 0.24	1.58 ± 0.08	3.3 ± 0.1	0.90 ± 0.02	1.67 ± 0.05	0.95 ± 0.03
LC21 (13.485)	Rhyolite	1.08 ± 0.33	1.27 ± 0.16	1.63 ± 0.22	3.3 ± 0.2	0.90 ± 0.04	1.70 ± 0.15	0.94 ± 0.05

concentrations with Nb between 9 and 12 ppm (Fig. 4). The Light Rare Earth Element Ratio to Heavy LREE to HREE ratio (La/Y) is 0.7–0.9.

Sample LC21 (0.940) was taken from the bottom 1 cm of the 22.4 cm thick dark grey to black tephra close to the top of core LC21. It is possible that this sample does not represent the full range of geochemistry of the tephra deposit as shown by studies elsewhere (e.g. the Campanian Ignimbrite of Tomlinson et al. (2012)). However, it should represent the first erupted component of the eruption as it was the first to be deposited. The shards are generally vesicular and often fluted in shape, show no evidence of chemical alteration, and often contain microphenocrysts.

The tephra shards in this sample are classified as rhyolitic on the basis of the total alkalis vs silica contents (Fig. 3) and the shards have a silica content of 73.73–74.92 wt%. FeOt content is 1.83–2.30 wt% and always higher than the CaO content which is 1.35–1.50 wt%. Na₂O (4.25–4.90 wt%) is higher than K₂O (3.17–3.49 wt%). The trace element concentrations from the LA-ICP-MS analyses show that the shards have relatively low HFSE concentrations (e.g. Nb 8.6–11.1 ppm, Zr ~176.5–301.6 ppm) and also that the Light Rare Earth Element to Heavy Rare Earth Element ratio (La:Y) is relatively low at 0.7–0.8. This sample is geochemically indistinguishable from sample LC21 (0.01), suggesting that the shards in LC21 (0.01) represent reworked shards from the visible tephra layer represented by sample LC21 (0.940).

Tephra LC21 (2.005). This sample lies just below sapropel 1 (Fig. 2). Tephra shards from this cryptotephra are constrained only within a 1 cm sample. The shards are platy and often fluted, but rarely have abundant vesicles and are free of microphenocrysts. They are clear in colour and show no evidence of chemical alteration.

The EPMA analyses of 34 of these tephra shards show that they are, as for LC21 (0.940), rhyolitic (Fig. 3). Similarly they also have FeOt (1.78–2.32 wt%) ~0.5 wt% higher than the CaO content (1.27–1.49 wt%) and Na₂O (4.31–5.25 wt%) is ~1 wt% higher than K₂O (3.07–3.49 wt%) (Fig. 4). LA-ICP-MS analyses of 19 of the shards shows that the sample has similar values of trace elements to LC21 (0.940) with HFSE concentrations of 9.3–11.8 ppm for Nb and 145–320 ppm for Zr. The LREE to HREE ratio is 0.7–0.8.

Tephra LC21 (3.225) is a sample from a peak of shard counts at the base of a 3 cm-deep region of cryptotephra in LC21 (Fig. 2). The shards are a mixture of platy and highly vesicular shards and contain abundant microphenocrysts. They do not appear to have been altered. The EPMA analyses provided wt% concentrations for forty shards and show that the sample can be classified as a rhyolite (Fig. 3). The shards have more FeOt than CaO, with larger ranges in these two elements than seen in the two samples discussed above (FeOt 0.79–4.98 wt%, CaO 0.8–3.29 wt%) (Fig. 4). K₂O values (2.84–3.81 wt% exceed N₂O values (2.85–5.06 wt%). LA-ICP-MS analysis was compromised by the number of micro-phenocrysts in the shards, and produced only five analyses of the trace element concentrations (Fig. 4). These five shards show Nb concentrations of 11.4–15.4 ppm and Zr values of 322–354 ppm, comparable to those of the previous two samples. The LREE to HREE ratio (Table 1) is approximately 0.63–0.72.

Tephra LC21 (3.775). This tephra sample was taken from the base of a peak in cryptotephra shards of >3000 shards/g (Fig. 2). The shards are generally fluted with occasional small vesicles and no evidence of geochemical alteration. 47 EPMA analyses attained for this sample classify this sample as a trachydacite/rhyolite (Fig. 3). CaO content (1.40–4.19 wt%) is generally lower than FeOt concentrations (2.62–5.22) and N₂O (3.12–6.05) is greater than K₂O (2.08–4.61) (Fig. 4). This sample has a relatively wide range of major element compositions and SiO₂ ranges from 66.03 wt% to 71.37 wt% (Fig. 3) 13 trace elements obtained by LA-ICP-MS yield HFSE concentrations (Fig. 4; Table 1) intermediate between the preceding three samples (described above) and LC21 (4.285) (described below). Nb concentrations are 13.6–16.6 ppm and Zr concentrations are 322–377 ppm (Fig. 4). The LREE to HREE ratio is 0.61–0.66.

Tephra LC21 (4.285) also is a sample from a peak in cryptotephra with concentrations of >3000 shards/g, spread over 2 cm (Fig. 2). The shards are often very small (<40 μm diameter) and have very large elongate vesicles within them, making them difficult to analyse using the available geochemical techniques. They do not show any evidence of geochemical alteration. The results of 11 EPMA measurements define the shards as rhyolitic (Fig. 3) and show that FeOt concentrations approximately equal CaO concentrations (1.34–2.11 and 0.97–2.17 wt% respectively). Na₂O content also approximately equals K₂O content (3.63–4.43 and 3.84–4.33 wt% respectfully) (Fig. 4). The shape and size of the glass surfaces on the shards made them impossible to analyse on the
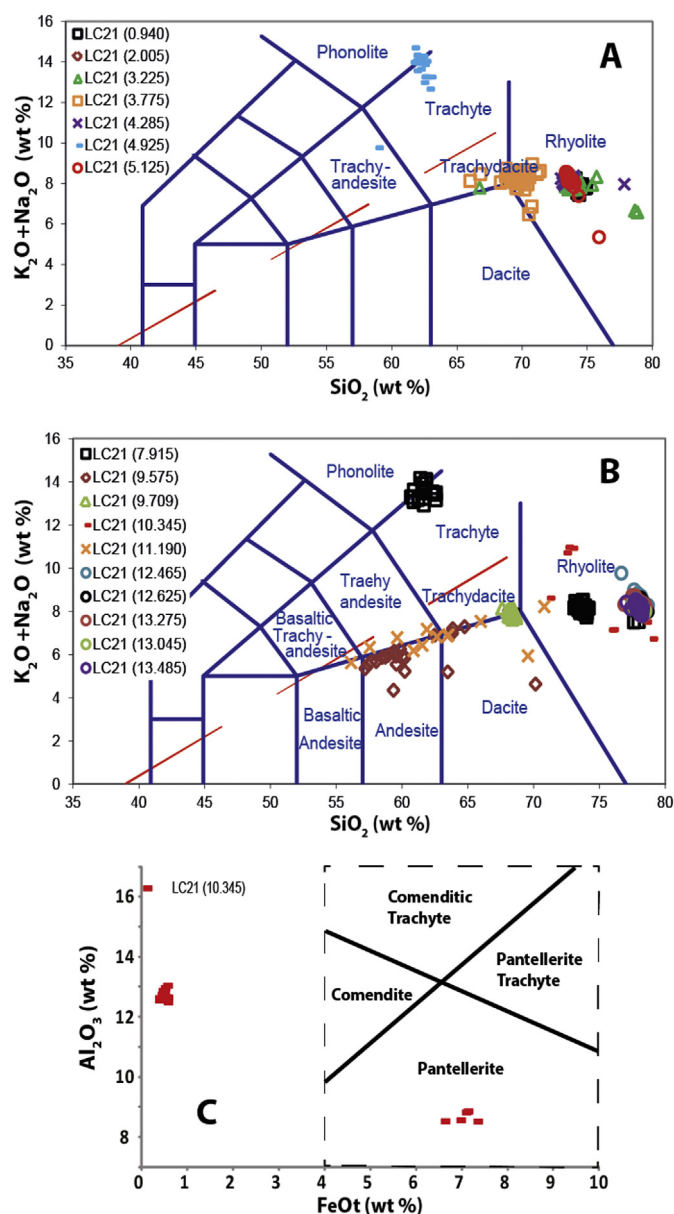
Fig. 3. Total Alkalis vs Silica diagrams (Le Bas, 1986) for the tephra samples described in LC21, arranged in stratigraphic order and divided for clarity into **A)** samples above sapropel 3, **B)** samples below sapropel 3, **C)** Al_2O_3 vs FeOt plot (after MacDonald, 1974) for sample LC21 (10.345) showing 5 shards which plot in the Pantellerite field. These samples from core LC21 are named with the depth in the core.

apparent lack of micro-phenocrysts did not guarantee abundant LA-ICP-MS results, for only five glass-only measurements were obtained (Fig. 4). Other analyses contained such abundant vesicle components that they had to be discarded. The five successful trace element determinations show very elevated HFSE concentrations (Nb 118.5–130.9 ppm, Zr 570–715 ppm) (Fig. 4), which are far in excess of those in the samples previously discussed.

Sample LC21 (5.125) is a 5 cm sediment sample with tephra shards (Fig. 2). When the core was re-sampled at 1 cm resolution, no shards were recovered. Possible explanations for this are: 1) the shards are contamination from another sample; 2) the shards did not form a laterally continuous layer across the core; 3) the tephra layer was laterally continuous, but was mostly removed by the saw when the core was cut into sections (this sample is the top sample in core section 8). In the first case, the tephra shards would be chemically and morphologically identical to those from another tephra layer found in the core, which was processed coevally with this sample. In the latter two scenarios, the shards would be geochemically different in some respect from those of the other tephra layers investigated.

The shards in this sample show no visible phenocrysts or evidence of chemical alteration. The EPMA analyses revealed 18 rhyolitic shards (Fig. 4) with SiO_2 values of 73.35–75.91 wt% and CaO values (1.32–1.52 wt%) lower than FeOt values (1.83–2.34 wt%). K_2O concentrations (3.25–3.54 wt%) are lower than Na_2O concentrations (1.97–5.27 wt%) (Fig. 4). The shards in this sample were mainly platy, but occasionally vesicular or fluted and all were clear in colour. Their platy morphology meant that when sectioned using cutting and polishing techniques it was difficult to expose large surfaces for trace element analysis with the LA-ICP-MS, and so the smaller beam of the SIMS was used for this sample. The five rhyolitic analyses show Nb values ranging from 10.9 to 23.0 ppm and Zr values from 308 to 407 ppm (Fig. 2). The La/Y (LREE to HREE ratio) is 0.7–0.8 (Table 1).

LC21 (7.915) is a sample from within sapropel S4a in LC21. The sample is taken from a peak in tephra shards of >3000 shards/g, and there are tephra shards in much lower concentrations in the 1 cm sample below this peak and 2 cm above the peak (Fig. 2). The shards are of mixed morphologies: some fluted, some platy and some highly vesicular. EPMA analyses revealed 17 trachyte/phonolitic shards and 38 rhyolitic shards (Fig. 3). The trachyte/phonolitic shards all have CaO lower in concentration than FeOt, and K_2O greater than Na_2O (Fig. 4). However, the trachyte/phonolitic component of this sample is bi-modal in its Na_2O composition, with one discrete mode containing $N_2O < 4.5$ wt% and the other >4.5 wt% (Fig. 4). The rhyolitic component (68–78 wt% SiO_2) has K_2O approximately 1 wt% higher than Na_2O and FeOt exceeds CaO by < 1 wt% (Fig. 4).

The 13 trace element analyses for the rhyolitic component of this sample show relatively low values of Nb 7–11 ppm and LREE to HREE ratios of between 0.7 and 2.4 (Fig. 4; Table 1).

Trace element analyses using the LA-ICP-MS were only possible on two of the trachyte/phonolitic shards, because these shards are in general thinner than the rhyolitic shards in this sample. Both of these shards were from the >4.5 wt% N_2O mode. They show Nb values of 92.8 and 104.4 ppm (Fig. 4), lower than observed in the visible trachyte/phonolite in LC21 (sample LC21–4.925), indicating that these shards are unlikely to be contaminants from that layer. Zr values are 463 and 413 ppm (Fig. 4). The LREE to HREE ratios for these two shards are 2.4 and 2.5 (Table 1).

LC21 (9.575) is the lowermost sample of many which contain >3000 shards/g of tephra in sapropel S5 in LC21 (Fig. 2). The tephra from this sample may not be representative of all the tephra in this section of the core. The shards are brown or clear in this sample, with rare phenocrysts, and can be either platy and vesicle-free or
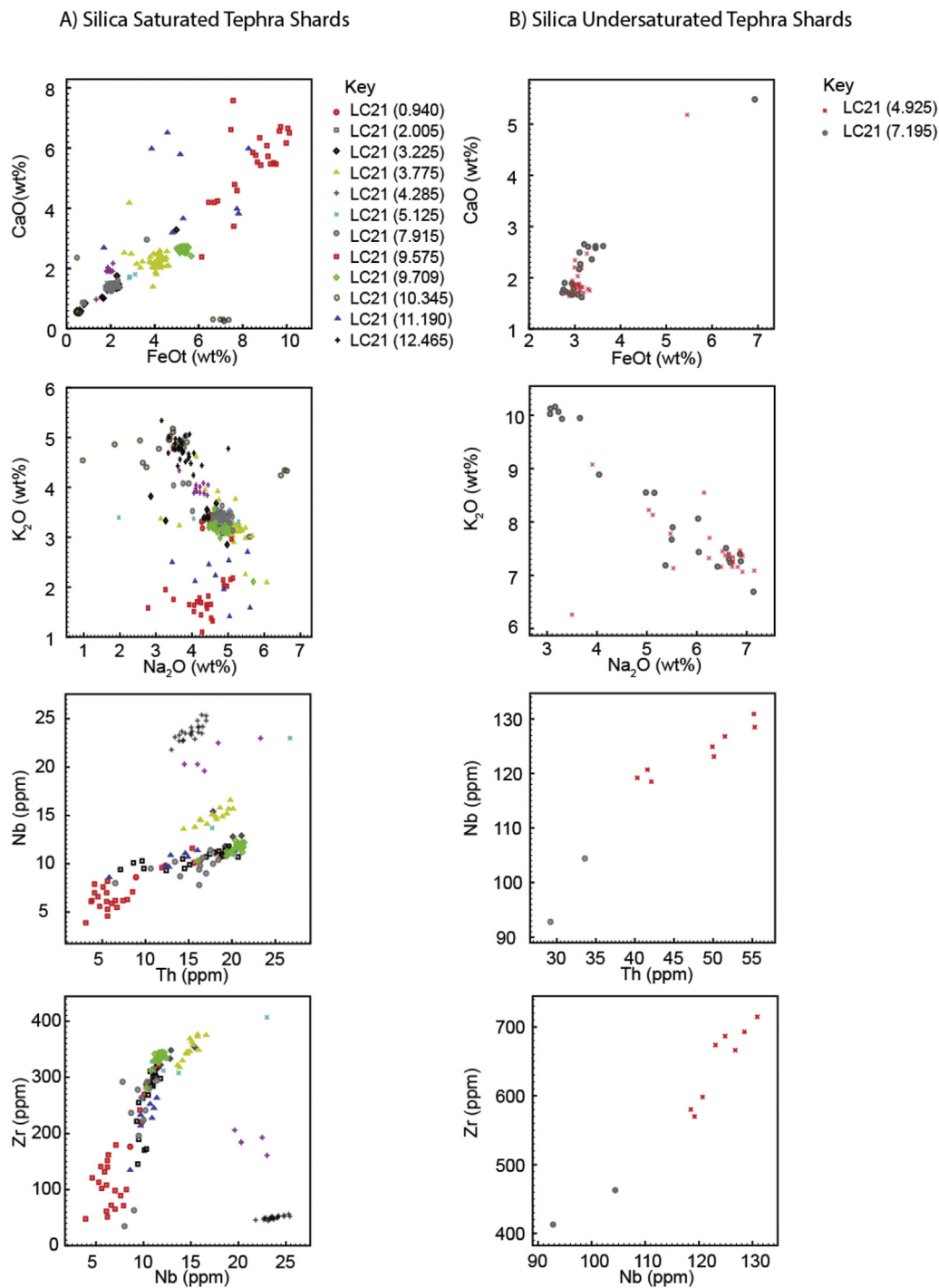
25 μm diameter LA-ICP-MS system but the 5 μm beam of the SIMS apparatus allowed five quantitative assessments of trace element concentrations. Nb ranges from 19.6 to 23.0 ppm (more enriched than all the samples previously described) while Zr is more depleted with values of 161–206 ppm (Table 1; Fig. 4) The LREE to HREE ratio is much higher than the previous samples, ranging from 1.9 to 2.3 (Table 1).

LC21 (4.925) is a sample from the base of the 15 cm-thick white tephra layer. The shards from this sample, which vary greatly in morphology (platy, fluted and highly vesicular shards) did not show any visible micro-phenocrysts and were all clear in colour. 24 EPMA results show that this tephra is a phonolite/trachyte (Fig. 3) and that its Na_2O values (3.50–7.15) are lower than the K_2O values (6.26–9.08). CaO is always lower in concentration than FeOt (1.64–5.18 wt% and 2.80–5.46 wt% respectively) (Fig. 4). The

Fig. 4. Selected bi-plots showing all tephra layers from LC21 A) Silica-Saturated shards from all tephra samples, and B) Silica-undersaturated shards from all tephra samples. All major element analyses from all samples are plotted in Supplementary Fig. 1, while all trace element analyses from all samples are shown in Supplementary Fig. 2. All analyses are provided in the Supplementary Data Table.

thicker with vesicles. The EPMA results reveal a wide range of SiO_2 values (57.19–70.14 wt%) classifying the shards as andesitic and dacitic (Fig. 3). Other major elements show a similarly large range in concentrations, although FeOt (4.17–10.12 wt%) is always more abundant than CaO (2.39–7.58 wt%), and Na_2O (2.77–5.11 wt%) is always greater than K_2O (1.08–2.96 wt%) (Fig. 4). The Nb (3.9–11.6 pmm) and Zr (48.0–322 ppm) values show a wide range (Fig. 4), in contrast to the LREE to HREE ratio (La/Y), which is consistently low (0.38–0.68) (Table 1).

LC21 (9.709) is a very thin (~1 mm) visible tephra layer within Sapropel S5 (Fig. 2). Its position in the sapropel makes it a potentially important stratigraphic marker for the correlation of LC21 to other sites. The tephra shards are generally platy with few vesicles or phenocrysts and no evidence of geochemical alteration. The EPMA results define the shards as trachydacite/dacitic with Ca concentrations of 2.41–2.74 wt%, always lower than the FeOt values of 5.01–5.67 wt% (Fig. 4). Na_2O values are consistently 4.45–5.68 wt% and higher than the 2.10–3.56 wt% K_2O values
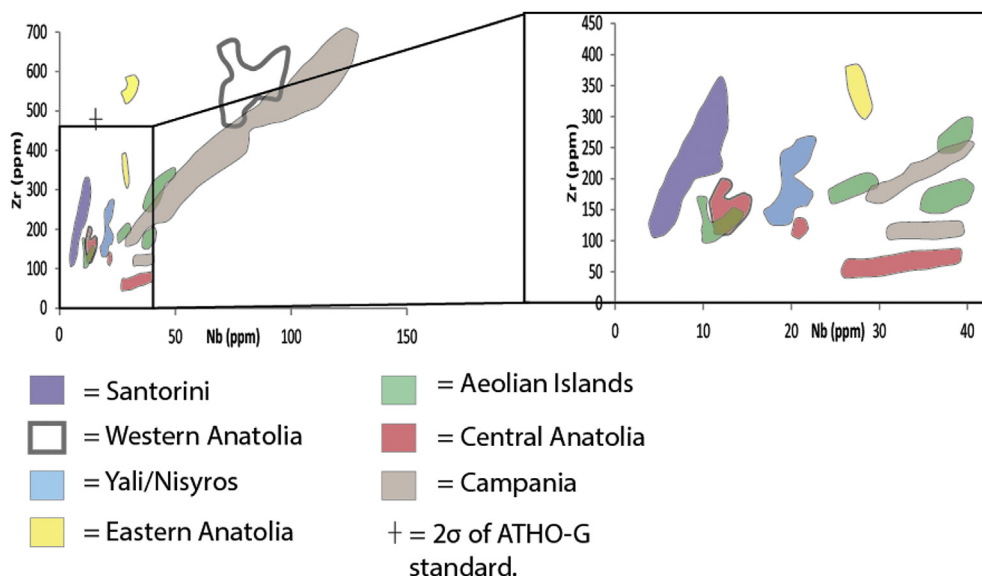
Fig. 5. Zr vs Nb data fields for proximal data from Santorini, Western Anatolia, Yali/Nisyros. Eastern Anatolia, Aeolian Islands, Central Anatolia and Campania showing that these elements effectively geochemically separate the sources, with the exception of the low Nb components of Central Anatolia and the Aeolian Islands.

(Fig. 4). These are relationships which appear to be consistent for all the silica-saturated samples discussed thus far for core LC21 (with the exception of LC21 4.285). The Nb content ranges from 4.4 to 12.2 ppm and Zr from 326 to 344 ppm (Fig. 4), which is also consistent with all the silica-saturated samples discussed so far for this core (with the exception of LC21–4.285). LREE to HREE (La/Y) ratios are confined to the range 0.50–0.53 for all the shards in this sample (Table 1).

LC21 (10.345) represents a peak in tephra shard concentrations of 2357 shards/g at the base of a 4 cm interval containing cryptotephra (Fig. 2). It contains both small platy shards and larger fluted shards. No shards contain significant vesicles or phenocrysts and none show evidence of alteration. The sample contains shards of high silica rhyolite (>77 wt% silica), and Pantellerite (>6% FeOt and <9% Al_2O_3) (Fig. 3). As the shards in this sample were all too small for LA-ICP-MS analysis, and because the major element concentrations of Pantellerite are distinctive, trace element data was not thought necessary to determine provenance. The shards with >77 wt% SiO_2 show $K_2O > Na_2O$ and differ from the other rhyolitic samples so far discussed in LC21. These shards also have very low FeOt and CaO values (<1 wt%) and the two elements are generally equal in abundance (Fig. 4).

LC21 (11.190) is a sample from the base of a 42 cm thick visible tephra below S5. The shards are highly vesicular. Nine EPMA analyses of the phenocryst-rich shards in this sample show that it has a highly variable chemistry ranging from 60.86 to 70.80 wt% SiO_2, classifying the shards as basaltic andesite to rhyolite (Fig. 3). The Na_2O values (3.44–5.59 wt%) are always in excess of the K_2O (1.40–2.70 wt%) values but there is no consistent difference in the abundance of CaO (2.70–6.52 wt%) and FeOt (1.69–8.26 wt%) (Fig. 4). The abundant phenocrysts meant that LA-ICP-MS analyses often contained mineral components. Only 6 pure glass trace element analyses could be achieved for this visible tephra, which show Nb values of 8.6–11.4 ppm, Zr values of 135–264 ppm and consistent La/Y ratios of 0.53–0.58 (Fig. 4; Table 1).

Tephras LC21 (12.465), (12.625), (13.275), (13.405) and (13.485). These 5 visible tephras are all contained within the lowermost section of LC21. The sediment between and above all 5 is very rich in tephra shards (>10,000 shards). In addition the lower 4 tephra layers are all inclined within the core and not laterally

continuous, indicating that they may be reworked by a physical process such as slumping. All five layers have platy shards and are phenocryst-free. The elemental abundances determined by EPMA (Supplementary Fig. 1) and LA-ICP-MS (Supplementary Fig. 2) are identical for all 5 samples and so they are described concurrently here.

The 140 EPMA for these five samples reveal a very homogenous major element composition; all are classified as high-silica rhyolites (>77% SiO_2) (Fig. 3) and have very low and virtually equal CaO and FeOt values (0.49–0.72 wt% and 0.36–0.75 wt%) (Fig. 4). K_2O (4.11–5.06 wt%) is always greater than Na_2O (3.15–4.99 wt%) (Fig. 4).

The micro-phenocryst-free nature of the samples also facilitated LA-ICP-MS analysis with 113 results obtained that show Nb concentrations varying between 16.5 and 26.8 ppm, while Zr concentrations range between 27.3 and 56.4 ppm (Fig. 4). The LREE to HREE (La/Y) ratio is consistently 1.5–2.0 (Table 1).

6. Geochemical comparison of LC21 tephra samples to proximal deposit samples

The aim of this paper is to define which volcanic sources have contributed to the tephrostratigraphy of marine core LC21. To this end, the geochemistry of the tephra shards has been compared to a large geochemical database created using samples taken directly from the major volcanic sources of the region (Tomlinson et al., 2012, 2014). Details of the database can be found at: http://c14.arch.ox.ac.uk/reset/embed.php?File=links.html and the volcanic sources are shown on Fig. 1. These volcanic sources are most clearly distinguished from one another using a Zr vs Nb plot (Fig. 5), an approach used previously by Clift and Blusztajn (1999). Thus, the LC21 tephra shards for each sample are plotted onto a Zr vs Nb plot together with the fields defined by proximal data (Fig. 6) to aid identification of the source volcanoes. All major and trace element tephra shard analyses for LC21 are given in the Supplementary Information. It is important to note also that while this approach is the most robust available to determine the source of tephra shards, both proximal and distal tephra records for each volcanic centre may be incomplete. Deposits originating from minor eruptions may have been eroded
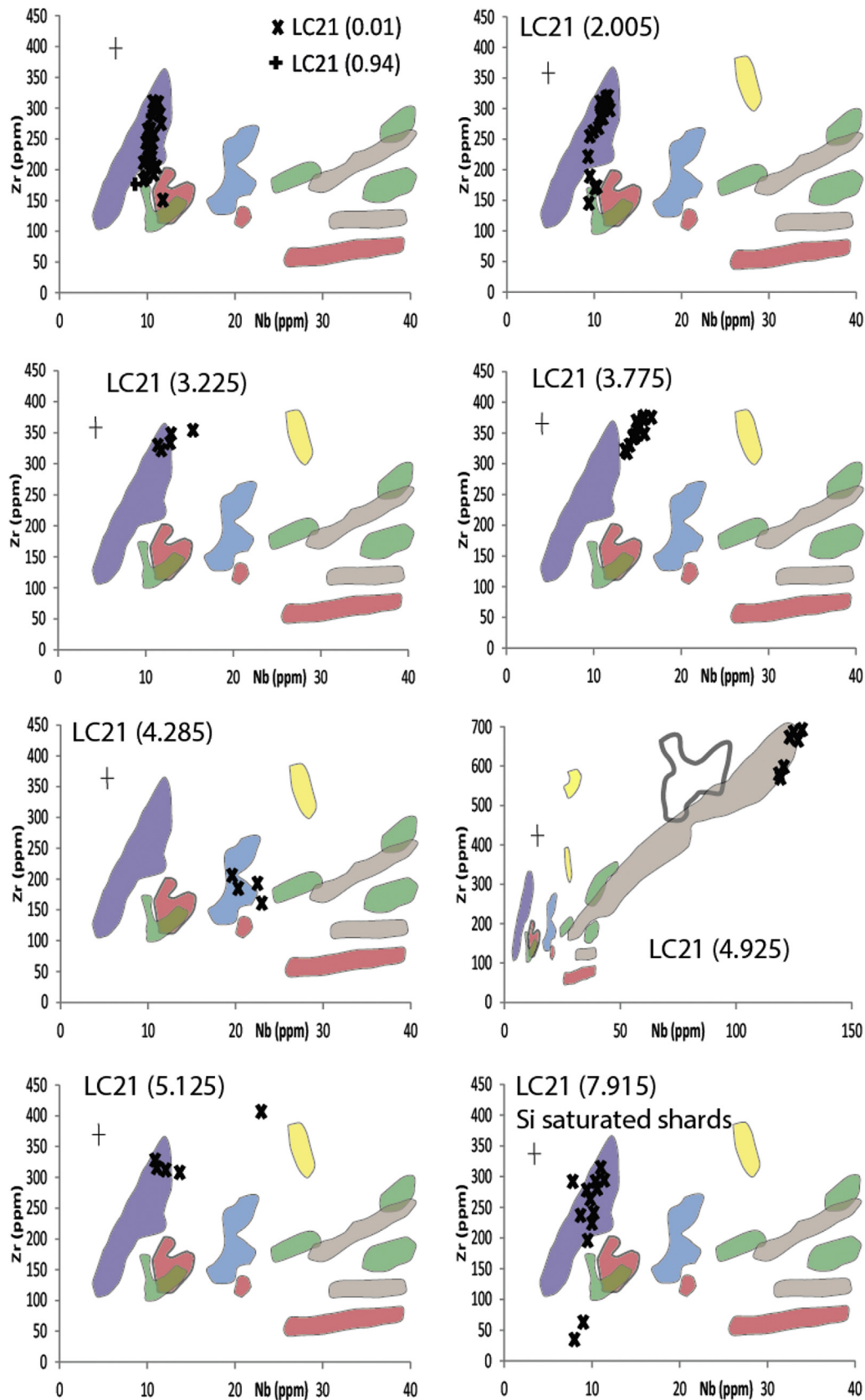
Fig. 6. Tephra shards from the samples taken in LC21, plotted on HFSE-Zr-Nb plots (after Clift and Blusztajn, 1999) with geochemical fields defined by the proximal volcanic deposits of the Mediterranean (Fig. 1): Santorini (Greece), Yali + Nisyros (Greece), the Aeolian Islands (Italy), Central Anatolia and Eastern Anatolia (Turkey), and Campanian Region (Italy). These are detailed on the RESET database and in Tomlinson et al. (2012), Albert et al. (2012, in press). As sample LC21 (7.915) contains both silica saturated and silica under-saturated shards these two populations cannot originate from the same eruption and thus are plotted on separate charts. These plots can be used to infer the most likely source system for the tephra shards found within the samples taken from LC21.
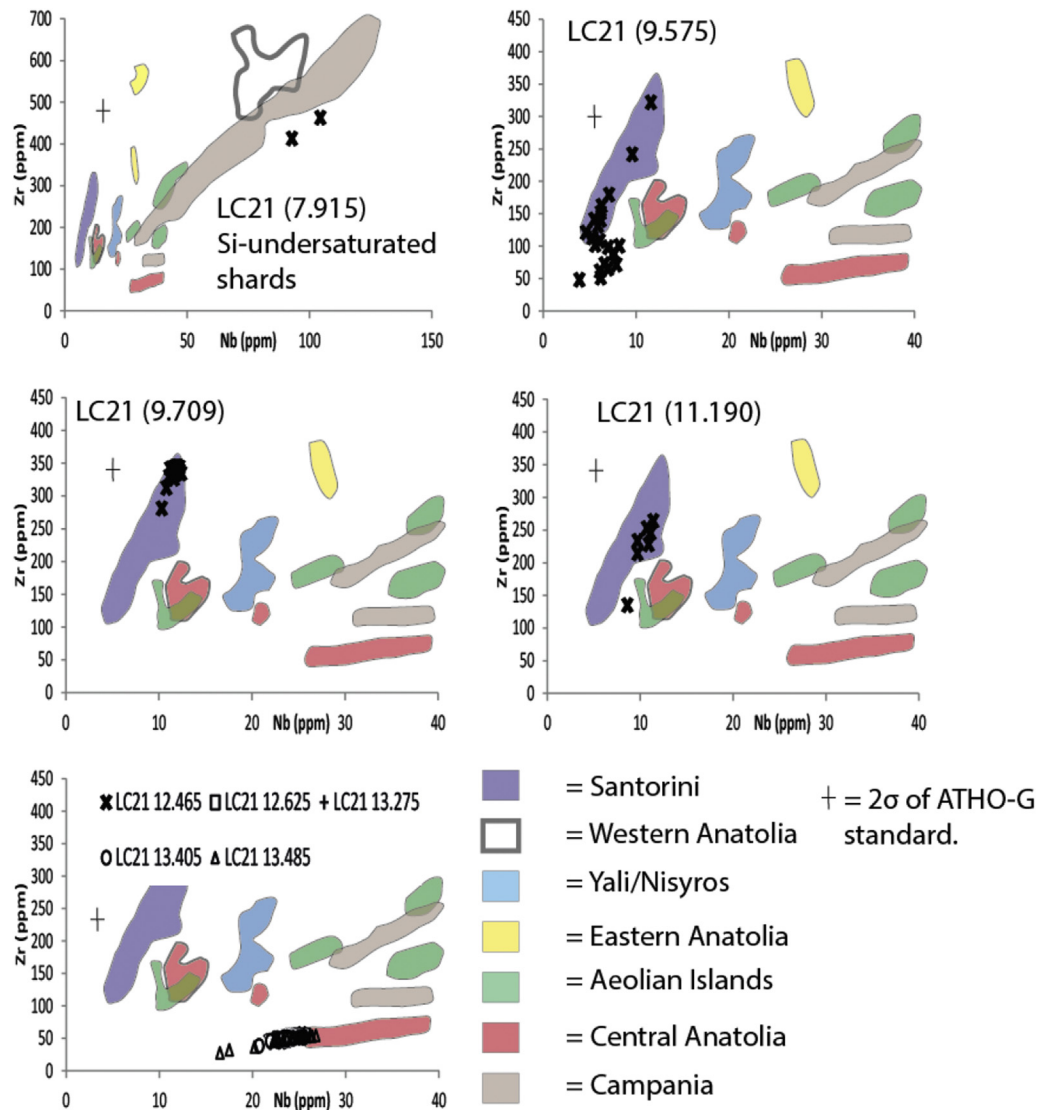
Fig. 6. (*continued*).

from proximal localities or may not have been deposited at all in a distal site.

Tephra LC21 (0.01 and 0.940) is the uppermost tephra layer represented in LC21. Sample LC21 (0.01) likely represents the reworked (by bioturbation, Watkins et al., 1978) shards in the sediment above the visible layer (Fig. 2), while LC21 (0.940) is from the base of the visible tephra layer. The majority of the data are similar to proximal tephras from Santorini (Fig. 6). Some analyses fall outside of the field of proximal data defined for Santorini. If these shards also originate from Santorini then they represent magmatic chemistries not represented by the available proximal database. Alternatively these shards could originate from another volcanic source or possibly Central Anatolia or the Aeolian Islands (Fig. 6), which was active within the period represented by these samples. This is however inconsistent with the ratios of the immobile elements (Nb/Y-Fig 7) and the large volume of tephra in this visible layer, which has already been attributed to the Minoan eruption of Santorini (Rohling et al., 2002b) based on radiocarbon dating. It should be noted, however, that some shards in the LC21 visible layer have geochemical spectra not currently represented in Santorini proximal deposits, including deposits of the Minoan eruption. This might indicate both that tephra deposits originating

from a single eruption may not have been geochemically homogeneous and that the full compositional range may be missing from proximal deposits. Heterogeneity has been observed previously in the deep sea deposits within the Santorini Caldera (Vinci, 1984), but was not in that study attributed to the Minoan eruption.

Tephra LC21 (2.005) is stratigraphically below the Minoan deposit. It is a potentially important marker for (marine) stratigraphic correlation because it is found just below sapropel S1 in LC21 (see Fig. 2). As with samples (0.01 and 0.940), the majority of the results obtained from this sample plot within the Santorini field (Fig. 6). Three of the shards are outside this field; one outside all the proximally defined fields, and two within the Aeolian Islands field. Therefore, the shards in this sample are either derived from Santorini and one or more other sources, or all originate from Santorini, but this again would imply that the proximal database for Santorini does not capture the full range of geochemical compositions. The latter is considered the most likely given (a) the geochemical similarity of this sample to the Minoan deposit in LC21 (sample LC21 (2.005), Fig. 4), (b) the fact that the proximal database comprises only the major Plinian eruptions, and (c) that the Nb/Y plot (Fig. 7) which shows the data from this sample plot closest to the Santorini field. This interpretation is tentative because, despite
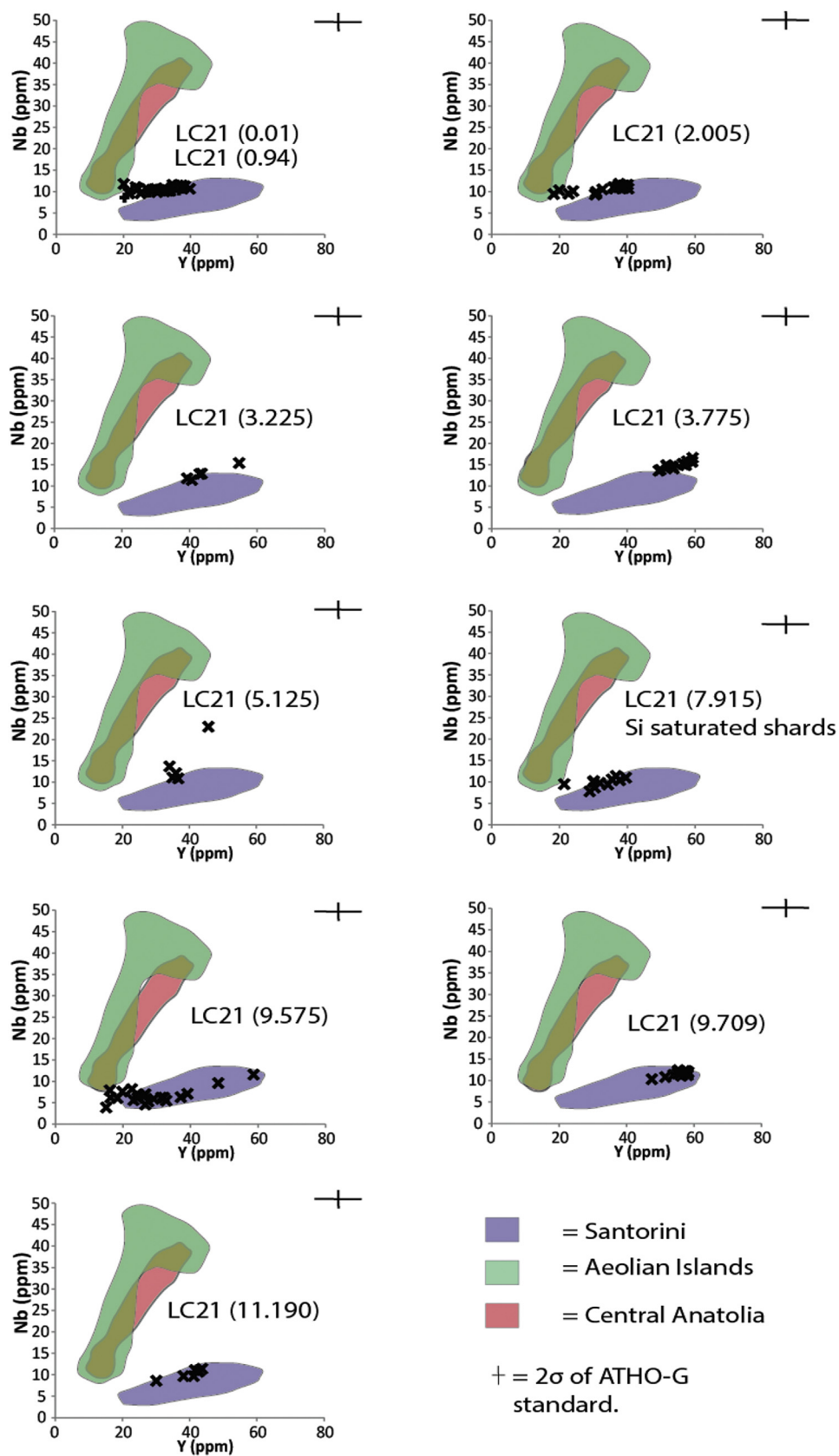
Fig. 7. Nb vs Y diagram to further distinguish the geochemistry of Santorini derived volcanic deposits from those of Central Anatolia and the Aeolian Islands. Plotted with these proximally derived fields are the analyses of samples which, from Fig. 6, are inferred to originate from Santorini.
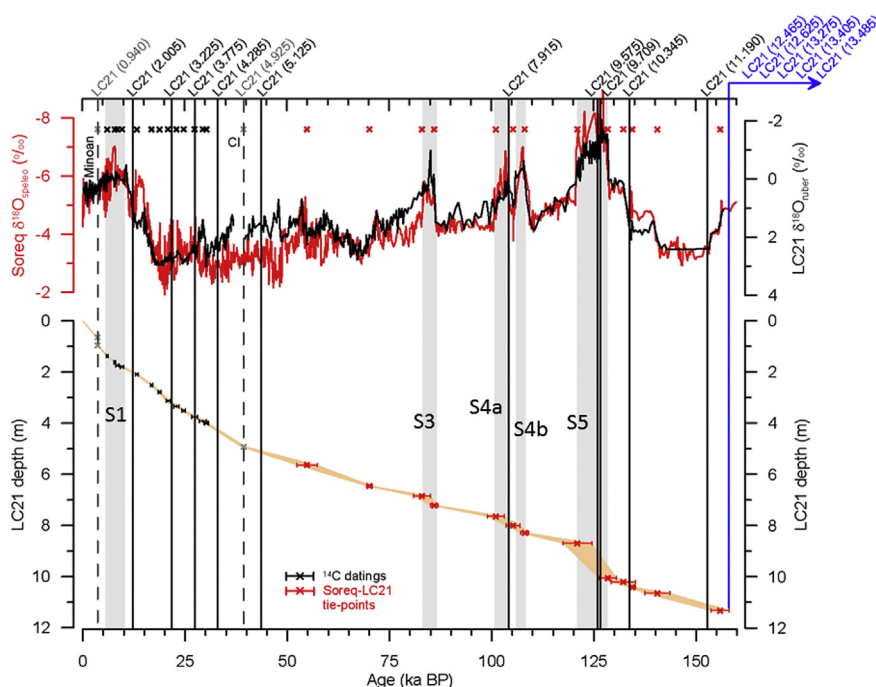
Fig. 8. Age model for LC21 (after Grant et al., 2012) constructed by correlating the δ¹⁸O_ruber isotope stratigraphy to the Soreq cave (Bar-Matthews et al., 2000). Black crosses indicate radiocarbon dates while red crosses indicate tie-points between the isotope stratigraphies. The error range of the age model is shown by the orange band. Tephra layers are shown by vertical black lines, sapropels are shown as grey vertical bands and labelled S1, S3, S4a, b and S5. The Minoan (LC21 0.940) and Campanian Ignimbrite (LC21 4.925) tephras were used in the construction of the age model and are shown by dotted vertical lines. Dates for the tephras, as defined from this age model (with the exception of LC21 0.940 and 4.925), are given in Table 1. Tephra layers older than the period represented by the age model are shown here in blue. The reader is referred to Grant et al. (2012) for details of the construction of the age model (including the calculations of sedimentation rates) through the correlation of the LC21 isotope stratigraphy with that of Soreq cave. (For interpretation of the references to colour in this figure legend, the reader is referred to the web version of this article.)

detailed sampling, Druitt et al. (2012) found no lavas or silicic pumice layers preserved between the Minoan deposits and those of the Cape Riva eruption of 22,329–21,088 BP (Lee et al., 2013). Rhyolitic tephra layer LC21 (2.005) is dated by the age model of Grant et al. (2012) (Fig. 5) to between 12.018 ± 0.349 and 12.143 ± 0.346 ka BP (Fig. 8; Table 2). It may therefore be evidence of rhyolitic eruptions from Santorini occurring between the Cape Riva and Minoan eruptions. Intriguingly, St Seymour et al. (2004) came to the same conclusion for a rhyolitic tephra layer (PhT1) dated by calibrated radiocarbon to 12.300–11.357 ka BP, in the Philippi peat basin of Northern Greece.

Tephra LC21 (3.225) is a rhyolite (consistent with an origin from Santorini) and nearly identical in chemical composition to LC21 (2.005) (Fig. 4). While one of the data points lies outside all of the geochemical fields (defined by the proximal data in Figs. 6 and 7, Tomlinson et al., 2014), the other four lie within the Santorini field. The rhyolitic classification of all shards (Fig. 3) is also consistent with an origin from Santorini. LC21 (3.225) is stratigraphically well below a calibrated AMS ¹⁴C date of ~17,000 cal BP at 2.525 m depth (Casford et al., 2007). The age model of Grant et al. (2012) suggests a date of between 21.653 ± 0.575 and 21.751 ± 0.581 ka BP (Fig. 8; Table 2) for LC21 (3.225). Vinci (1985) attributes a tephra layer of similar SiO₂ content, stratigraphically immediately below the Cape Riva tephra (Fig. 9) in marine cores MC7 and MC12 (Southern Aegean Sea), to Santorini, but could not find a matching proximal deposit, supporting the proposal that there are tephra layers preserved in Aegean sediments that are not yet represented in the proximal geochemical database.

Tephra LC21 (3.775) has a different chemical composition to LC21 (3.225), being significantly lower in SiO₂ (~70%) (Fig. 3). The compositions of these rhyolitic shards plot outside all of the proximally-defined data fields (Figs. 6 and 7). The shards in this

sample therefore originate from either a rhyolitic volcano considered here (but a composition absent from our proximal database) or from another volcano not considered in this study. The former interpretation is preferred as one analysis from the Santorini-assigned sample LC21 (3.225) plots amongst the shards from sample LC21 (3.775) (Fig. 4) which is itself attributed to Santorini. This tephra layer may represent a minor rhyolitic eruption from Santorini. The LC21 age model gives an age of between 27.481 ± 0.719 and 27.354 ± 0.706 ka BP (Fig. 8; Table 2).

Tephra LC21 (4.285) lies stratigraphically above the Campanian Ignimbrite (CI) deposit (see LC21 (4.925) below and Lowe et al., 2012). Fig. 6 indicates a source from the Yali or Nisyros centres. The rhyolitic chemistry of the shards in this sample (Fig. 3) is consistent with both of these sources. The LC21 age model (Fig. 5) suggests an age for LC21 (4.285) of between 32.894 ± 0.502 and 32.992 ± 0.503 ka BP (Table 2). The Yali-2 tephra has been identified as a visible layer in cores KB-33 (Vinci, 1985) and MAR-03-24 (Aksu et al., 2008) (Fig. 9) both to the South East of the island of Yali, and in various cores up to 300 km south-east of the island by Federman and Carey (1980) as well as proximally to the island (Allen and McPhie, 2000). Tephra attributed to the major Nisyros eruptions of the Upper and Lower Pumices has been located in ocean cores in the Central Aegean (Hardiman, 1999; Aksu et al., 2008) and on Lesvos Island to the North of Nisyros (Margari et al., 2007). This study is therefore the first to discover crypto-tephra originating from one of these sources, extending the known footprint of these two volcanoes to approximately 100 km southwest of the islands (Fig. 1).

Tephra LC21 (4.925) represents a visible layer of 13 cm thickness. The glass shards are phonolitic in composition (Fig. 3a) and lie in the Campanian geochemical composition field (Smith et al., 2011; Tomlinson et al., 2012, 2014) in Fig. 6. This tephra layer has

Table 2
Summary of the tephra samples from LC21, their likely source and estimated age from the LC21 age model of Grant et al. (2012).

Tephra name in LC21	Sample depth (mbsf in LC21)	Thickness of layer (Fig. 2)	TAS classification (from Fig. 3).	HFSE source inference (Figs. 6 and 7)	Date (ka) for tephra sample from LC21 age model (Fig. 8)
LC21 (0.01)	0.01—0.00	Crypto-tephra	Rhyolite	Santorini	NA
LC21 (0.940)	0.940—0.716 m	22.4 cm	Rhyolite	Santorini	Published age of 3344.9 ± 7.5 ka used to define age model
LC21 (2.005)	2.005—1.995 m	Crypto-tephra from 1 cm peak concentrations	Rhyolite	Santorini	Top = 12.018 ± 0.349 Base = 12.143 ± 0.346
LC21 (3.225)	3.225—3.215 m	Crypto-tephra from 1 cm peak concentrations	Rhyolite	Santorini	Top = 21.653 ± 0.575 Base = 21.751 ± 0.581
LC21 (3.775)	3.775—3.765 m	Crypto-tephra from 1 cm peak concentrations	Trachydacite/Rhyolite	Santorini	Top = 27.354 ± 0.706 Base = 27.481 ± 0.719
LC21 (4.285)	4.285—4.275 m	Crypto-tephra from 1 cm peak concentrations	Rhyolite	Kos/Yali/Nisyros	Top = 32.894 ± 0.502 Base = 32.992 ± 0.503
LC21 (4.925)	4.925—4.795 m	13 cm	Phonolite/Trachyte	Campania	Published age of 39,300 ± 110 ka Used to define age model (De Vivo et al., 2001)
LC21 (5.125)	5.125—5.075 m	Crypto-tephra from 5 cm sample	Rhyolite	Santorini	Top = 42.532 ± 1.015 Base = 43.617 ± 1.159
LC21 (7.915)	7.915—7.905 m	Crypto-tephra from 1 cm peak concentrations	Rhyolite and Phonolite/Trachyte	Santorini and Campania	Top = 103.980 ± 2.020 Base = 104.100 ± 2.050
LC21 (9.575)	9.575—9.565 m	Crypto-tephra from 1 cm peak concentrations	Andesite/Dacite/ Trachydacite	Santorini	Top = 125.653 ± 2.829 Base = 125.708 ± 2.819
LC21 (9.709)	9.709—9.707 m	0.2 cm	Dacite/Trachydacite	Santorini	Top = same as base Base = 126.440 ± 2.691
LC21 (10.345)	10.345—10.335 m	Crypto-tephra from 1 cm peak concentrations	Pantellerite and Rhyolite	Pantelleria (from Ca vs Fe plot) and possibly Kos/Yali/ Nisyros from high SiO_2	Top = 133.469 ± 2.000 Base = 133.573 ± 1.911
LC21 (11.190)	11.190—10.770 m	42 cm	Basaltic Andesite to Rhyolite	Santorini	Top = same as base Base = 152.588 ± 9.324
LC21 (12.465)	12.345—12.465 m	12 cm	Rhyolite	Kos/Yali/Nisyros	>152.58
LC21 (12.625)	12.610—12.625 m	1.5 cm	As above	As above	As above
LC21 (13.275)	12.225—13.275 m	2 cm	As above	As above	As above
LC21 (13.405)	13.365—13.204 m	4 cm	As above	As above	As above
LC21 (13.485)	13.440—13.485 m	4.5 cm	As above	As above	As above

previously been identified as the widespread Campanian Ignimbrite (CI) tephra (Lowe et al., 2012). The CI has been $^{39}Ar/^{40}Ar$ dated to 39.28 ± 0.11 ka BP (De Vivo et al., 2001), the date incorporated into the LC21 age model (Fig. 8) and thus no independent age estimate can be derived for this tephra layer. The CI is arguably the most widespread and intensively studied tephra layer in the Mediterranean region (Fig. 9) (e.g. Seymour and Christanis, 1995; Pyle et al., 2006; Costa et al., 2012; Lowe et al., 2012; Tomlinson et al., 2012).

LC21 (5.125) shards were recovered from the 5 cm resolution sampling series only, and not from the 1 cm sampling. As the sample is the top 5 cm of a core section, it is possible that some of the tephra layer was removed during the shipboard dissection of the core (only 101 shards were counted in the 5 cm sample; Fig. 2). LC21 5.125 contains rhyolites with geochemical similarities to Santorini (Figs. 6 and 7), to which it is tentatively assigned, and is dated by the Grant et al. (2012) age model to between 42.532 ± 1.015 and 43.617 ± 1.159 ka (Table 1).

LC21 (7.915) contains both sub-alkaline and alkaline components (Fig. 3). The majority of the sub-alkaline (rhyolitic) shards are chemically similar to the proximal data of Santorini (Figs. 6 and 7) and are therefore inferred to originate from eruptions on the island. Three of the sub-alkaline shards do not, however, plot within any of the proximal fields (Figs. 6 and 7). Whatever their origin, they share the same eruption date (within sample resolution) as the alkaline component of the same sample.

The two trace element analyses of the alkaline shards are closest in composition to Campanian data-fields (Fig. 6) and their phonolitic composition is also consistent with a Campanian source. Their alkaline major element compositions also accord with those of

LC21 (4.925) (Fig. 4) which has been identified as the Campanian Ignimbrite tephra layer. LC21 (7.915) is dated to between 103.980 ± 2.020 and 104.100 ± 2.050 ka BP by the LC21 age model (Fig. 8; Table 2). It may therefore relate to the widespread X-5 or X-6 tephra layers identified in the Central Mediterranean (Wulf et al., 2004; Bourne et al., 2010; Vogel et al., 2010; Wulf et al., 2012), which are $^{40}Ar/^{39}Ar$ dated to 106.2 ± 1.3 ka BP (Giaccio et al., 2012) and 108.9 ± 1.8 ka BP (Iorio et al., 2014), respectively.

LC21 (9.575) is a sample from the base of a rich layer of crypto-tephra in the core (Fig. 2) and lies within sapropel 5 (S5). The exaggerated thickness of S5 in LC21 (Marino et al., 2007) and the increased sedimentation rate in this part of the core (Fig. 5) may be partly due to the input of tephra into the core site at this time. Nine shards from this sample have chemical compositions that fall within the field defined by the Santorini proximal data (Figs. 6 and 7). Their andesitic to dacitic chemistry is also consistent with this source. However 11 shards with sub-alkaline chemistry plot outside all proximally-defined geochemical fields on Fig. 6. Together with the large volume of tephra represented in this part of the core, by an origin from Santorini, Kos, Yali or Nisyros, which are the closest volcanic sources, seems more likely (Fig. 1). The sample is dated by the LC21 age model to between 125.653 ± 2.829 and 125.708 ± 2.819 ka (Fig. 8; Table 2).

LC21 (9.709) is a visible (Fig. 2), silica-saturated tephra layer within sapropel S5. All shards from this sample have a rhyolitic chemistry and plot within the Santorini field (Figs. 6 and 7) and are thus inferred to originate from the island. The sample is dated at 126.440 ± 2.691 ka BP by the Grant et al. (2012) age model (Table 1).

LC21 (10.345) contains Pantellerite shards (Fig. 3), which the LC21 age model dates to between 133.469 ± 2.000 and
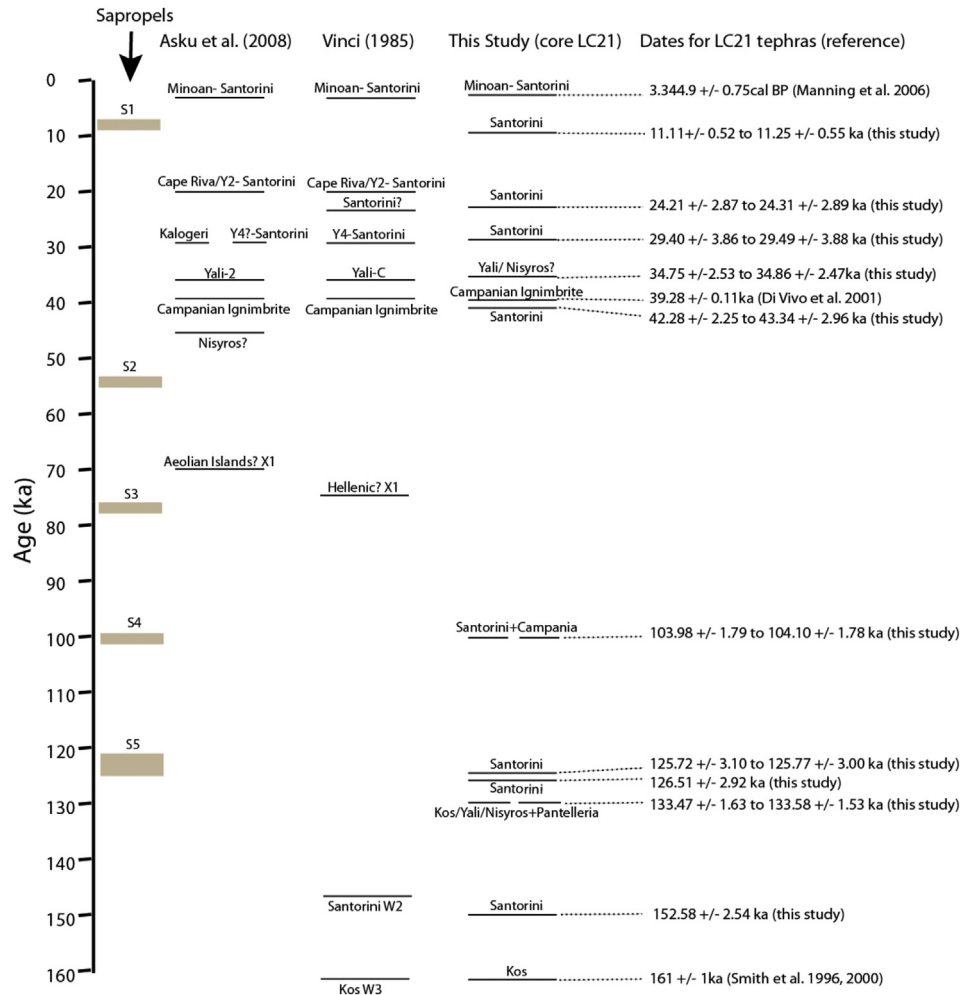
Fig. 9. Marine tephrostratigraphies in the Aegean region as reported by Aksu et al. (2008), Vinci (1985) and this study. Volcano or eruption attributions assigned to tephra layers are those assigned by the original work of Aksu et al. (2008), Vinci (1985) and this study respectively. No correlations between these stratigraphies are presented as these have not been presented or tested in this paper. Sapropel layers are shown for stratigraphic guidance on the left; labelled S1–S5.

133.573 ± 1.911 ka BP (Fig. 8; Table 2). Three tephra layers approximating this date and originating from Pantelleria have been identified in the Ionian Sea (Tamburrino et al., 2012) and LC21 (10.345) may relate to one of these layers. Pantellerian tephra has also been found on the island of Lesvos (Margari et al., 2007) and in Lake Ohrid in Albania (Vogel et al., 2010), so this new discovery of Pantellerian tephra shards in a marine core in the Aegean Sea raises the prospect of a widespread tephra isochron in the region.

The second geochemical component of LC21 (10.345) is a high SiO_2 rhyolite (Fig. 3). Although no trace element data could be obtained from this sample, the very high SiO_2 values (76–78%) suggest these shards may originate from the Kos/Yali/Nisyros system (Bachmann et al., 2007).

LC21 (11.190) is taken from the base of a 42 cm thick visible tephra layer with a very broad major element composition ranging from basaltic andesite to rhyolite (Fig. 3). All but one of the shards plot within the geochemical field defined by Santorini proximal deposits (Fig. 6), the single outlier plotting outside of all proximal fields in the reference database. The silica saturated classification (Fig. 3) of all shards in this sample also supports an attribution to Santorini. This distal tephra layer has a date of 152.588 ± 9.324 ka BP as defined by the LC21 age model (Fig. 8; Table 2). It may therefore correlate to the Middle Pumice eruption of Santorini (W2) (Fig. 9), which has an estimated date of ~150 ka BP based on sapropel chronology (Vinci, 1985).

Tephras LC21 (12.465), (12.625), (13.275), (13.405) and (13.485) are all chemically indistinguishable (Supp. Figs. 1e and 2e) and span a tephra-rich region at the base of the core (Fig. 2). The HFSE plot (Fig. 6) suggests these tephras might originate from the central Anatolian volcanic centre as, geochemically, this is the closest field. However, the distance to this source of >700 km combined with the thickness (up to 10 cm) of these layers (Fig. 2) makes these two lines of evidence difficult to reconcile. It is therefore suggested that, given the unusually high silica contents for the shards in these samples (Fig. 3), their probable source is Kos, the one local volcanic source that is absent from the proximal database used here. Kos shares the characteristic of producing highly silicic (>75 wt% SiO_2) magmas with its neighbour Nisyros (Bachmann et al., 2010). Kos also produced a Plinian caldera-forming eruption at 161 ka BP (Smith et al., 1996, 2000) which is consistent with the stratigraphic position of these tephra layers below sapropel S5 (dated at ~128–121 ka BP by Grant et al., 2012) (Fig. 9). In addition the physical reworking evident in this lowermost section of the core may be a result of seismic activity occurring coevally with caldera formation. The data presented here are therefore thought to be the first published major and trace element data derived from glass assigned to this important eruption – the Kos Plateau Tuff. Major and trace element analyses of proximal Kos Plateau Tuff deposits are needed to test this assertion.

Fig. 9 summarises the full LC21 tephrostratigraphic record and sets this against the published stratigraphies of Aksu et al. (2008) and Vinci (1985). It has been demonstrated that distal tephra deposits in the Aegean Sea are most likely derived from Santorini, the Kos/Yali/Nisyros system, the Campanian System and Pantelleria. Age estimates for the tephras, based on the LC21 chronology (Table 1), are shown on Fig. 9.

7. Conclusions

The tephrostratigraphical results reported here for marine core LC21 represents the longest single-core record of volcanic activity obtained from marine sediments of the Eastern Mediterranean region, and the first to include detection of cryptotephra layers. Of the 17 discrete tephra layers detected in the sequence, a number have very similar chemical compositions, but can be differentiated and ordered stratigraphically by position relative to: (a) compositionally distinctive tephra layers - the Minoan Tephra, the Campanian Ignimbrite, a Pantelleria-sourced eruption, and the Kos Plateau Tuff eruption; (b) sapropel layers S1—S5; and (c) a well-resolved isotope-based chronostratigraphy (Grant et al., 2012). Eight of the 17 tephra layers are non-visible cryptotephra layers, and these collectively suggest that past studies of the volcanic records in the Aegean, which previously have focussed on visible tephra layers only, are incomplete.

Several of the tephra layers reported here have compositions most closely matching the proximal deposits of Santorini (also the closest source) of which three (LC21 (2.005), (3.225) and (3.775)) have chemical signatures not represented in the current proximal Plinian eruption database that includes Minoan, Cape Riva, Upper Scoria 1, Upper Scoria 2, Vourvolous, and Middle Pumice eruption material (Druitt et al., 1989, 1999; Tomlinson et al., 2014). It is therefore inferred that distal stratigraphic archives may preserve some of the inter-Plinian eruptions of Santorini (Vespa et al., 2006), in addition to the Plinian eruptions. More detailed investigations of both proximal and distal records in the region are needed to establish the magnitude of the eruptions that deposited the cryptotephra layers reported here.

This paper also presents the first evidence for Pantellerian tephra shards in the Aegean Sea (within LC21 (10.345)) and a large glass geochemical dataset LC21 (12.456, 12.625, 13.275, 13.405 and 13.485) which is likely to be attributable to the Plinian Kos Plateau Tuff (KPT) eruption (Smith et al., 1996, 2000; Bachmann et al., 2007, 2010). Pantellerian eruptive material has a distinctive chemistry, and tephras of a similar age with a Pantelleria source have previously been reported from the Island of Lesvos (Margari et al., 2007), Albania (Vogel et al., 2010) and sediments in the Ionian Sea (Tamburrino et al., 2012). This distinctive tephra layer therefore appears to offer potential as a late Quaternary marker for correlating sediment sequences within the Aegean and with neighbouring land records. The island of Kos is considered to be the likely source of the basal tephra layers reported from LC21. Unfortunately, these basal tephra layers appear to have been reworked, which compromises their interpretation. However, the LC21 record does reveal that the KPT reached this part of the Aegean in copious quantities and therefore may also provide a regional stratigraphic marker within other environmental records.

In addition to the Campanian Ignimbrite, the most widespread late Quaternary tephra in the Mediterranean region (e.g. Pyle et al., 2006; Costa et al., 2012), LC21 contains an older tephra with Campanian chemical composition (e.g. Tomlinson et al., 2012, 2014). It is considered most likely to equate with either the X-5 or X-6 tephra layers (Giaccio et al., 2012), but further work is required to confirm this. If the LC21 record can be successfully linked to the X5 or X6 tephra layers identified in sequences from

the Tyrrhenian and Adriatic Seas, this would provide a second independent, pan-Mediterranean chronological marker in addition to the CI.

The LC21 record therefore demonstrates the potential for enhancing the tephrostratigraphy of the eastern Mediterranean by including methods for detecting cryptotephra layers in routine site investigations. Much work remains to be done, however, to secure more confident comparisons between distal and proximal volcanic stratigraphies. The rewards may be high however, in two respects: (i) an increase in the number of tephra isochrons that can be for synchronising Pleistocene palaeoenvironmental records, and (ii) possible evidence of additional volcanic activity that is not at present represented in proximal volcanic records.

Appendix A. Supplementary data

Supplementary data related to this article can be found at http://dx.doi.org/10.1016/j.quascirev.2015.04.005.

References

Abu-Zied, R.H., Rohling, E.J., Jorissen, F.J., Fontanier, C., Casford, J., Cooke, S., 2008. Benthic foram response to changes in bottom-water oxygenation and organic carbon flux in the eastern Mediterranean during LGM to recent times. Mar. Micropaleontol. 67, 46—68.

Aksu, A.E., Jenner, G., Hiscott, R.N., Isler, E.B., 2008. Occurrence, stratigraphy and geochemistry of late Quaternary tephra layers in the Aegean Sea and Marmara Sea. Mar. Geol. 252, 174—192.

Albert, P.G., Tomlinson, E.L., Smith, V.C., Di Roberto, A., Todman, A., Rosi, M., Marani, M., Muller, W., Menzies, M.A., 2012. Marine-continental tephra correlations: volcanic glass geochemistry from the Marsili Basin and the Aeolian Islands, Southern Tyrrhenian Sea, Italy. J. Volcanol. Geotherm. Res. 229—230, 74—94.

Albert, P.A., Hardiman, M., Keller, J., Tomlinson, E., Smith, V.C., Bourne, A.J., Wulf, S., Zanchetta, G., Sulpizio, R., Müller, U.C., Pross, J., Ottolini, L., Matthews, I.P., Blockley, S.P.E., Menzies, M., 2014. Revisiting the Y-3 tephrostratigraphic marker: a new diagnostic glass geochemistry, age estimate and details on its climatostratigraphical context. Quat. Sci. Rev. http://dx.doi.org/10.1016/j.quascirev.2014.04.002 (in press).

Allen, S.R., McPhie, J., 2000. Water-settling and resedimentation of submarine rhyolitic pumice at Yali, eastern Aegean, Greece. J. Volcanol. Geotherm. Res. 95, 285—307.

Ascough, P., Cook, G., Dugmore, A., 2005. Methodological approaches to determining the marine radiocarbon reservoir effect. Prog. Phys. Geogr. 29, 523—547.

Bachmann, O., Charlier, B.L.A., Lowenstern, J.B., 2007. Zircon crystallisation and recycling in the magma chamber of the Kos Plateau Tuff (Aegean Arc). Geology 35, 73—76.

Bachmann, O., Schoene, B., Schnyder, C., Spikings, R., 2010. The $^{40}Ar/^{39}Ar$ and U/Pb dating of young rhyolites in the Kos-Nisyros volcanic complex, Eastern Aegean Arc, Greece: age discordance due to excess ^{40}Ar in biotite. Geochem. Geophys. Geosyst. 11, 1525—2027.

Bar-Matthews, M., Ayalon, A., Kaufman, A., 2000. Timing and hydrological conditions of Sapropel events in the Eastern Mediterranean, as evident from speleothems, Soreq cave, Israel. Chem. Geol. 169, 145—156.

Bar-Matthews, M., Ayalon, A., Gilmour, M., Matthews, A., Hawkesworth, C.J., 2003. Sea-land oxygen isotopic relationships from planktonic foraminifera and speleothems in the Eastern Mediterranean region and their implication for paleorainfall during interglacial intervals. Geochim. Cosmochim. Acta 67, 3181—3199.

Blockley, S.P.E., Pyne-O' Donnel, S.D.F., Lowe, J.J., Matthews, I.P., Stone, A., Pollard, A.M., Turney, C.S.M., Molyneux, E.G., 2005. A new and less destructive laboratory procedure for the physical separation of distal glass shards from sediments. Quat. Sci. Rev. 24, 1952—1960.

Bronk Ramsey, C., 2008. Deposition models for chronological records. Quat. Sci. Rev. 27, 42—60.

Bronk Ramsey, C., Housley, R.A., Lane, C.S., Smith, V.C., Pollard, A.M., 2014. The RESET database and associated analytical tools. Quat. Sci. Rev. http://dx.doi.org/10.1016/j.quascirev.2014.11.008.

Bourne, A.J., Lowe, J.J., Trincardi, A., Asioli, A., Blockley, S.P.E., Wulf, S., Matthews, I.P., Piva, A., Vigliotti, L., 2010. Distal tephra record for the last ca 105,000 years from the core PRAD 1—2 in the central Adriatic Sea: implications for marine tephrostratigraphy. Quat. Sci. Rev. 29, 3079—3094.

Casford, J.S.L., Rohling, E.J., Abu-Zied, R., Cooke, S., Fontanier, C., Leng, M., Lykousis, V., 2002. Circulation changes and nutrient concentrations in the late Quaternary Aegean Sea: a nonsteady state concept for sapropel formation. Paleoceanography 17, 14.1—14.11.

Casford, J.S.L., Rohling, E.J., Abu-Zied, R.H., Fontanier, C., Jorissen, F.J., Leng, M.J., Schmiedl, G., Thomson, J., 2003. A dynamic concept for eastern Mediterranean circulation and oxygenation during sapropel formation. Palaeogeogr. Palaeoclimatol. Palaeoecol. 190, 103—119.

Casford, J.S.L., Abu-Zied, R., Rohling, E.J., Cooke, S., Fontanier, C., Leng, M., Millard, A., Thomson, J., 2007. A stratigraphically controlled multiproxy chronostratigraphy for the eastern Mediterranean. Paleoceanography 22, PA4215.

Cassidy, M., Watt, S.F.L., Palmer, M.R., Trofimovs, J., Symons, W., Maclachlan, S.E., Stinton, A.J., 2014. Construction of volcanic records from marine sediment cores: a review and case study (Montserrat, West Indies). Earth Sci. Rev. 138, 137—155.

Cita, M.B., Vergnaud-Grazzini, C., Robert, C., Chamley, H., Ciaranfi, N., d'Onofrio, S., 1977. Paleoclimatic record of a long deep sea core from the eastern Mediterranean. Quat. Res. 8, 205—235.

Clift, P., Blusztajin, J., 1999. The trace-element characteristics of Agean and Aeolian volcanic arc rocks. J. Volcanol. Geotherm. Res. 92, 321—347.

Costa, A., Folch, A., Macedonio, G., Giaccio, B., Isaia, R., Smith, V.C., 2012. Quantifying volcanic ash dispersal and impact of the Campanian Ignimbrite super-eruption. Geophys. Res. Lett. 39, L10310. http://dx.doi.org/10.1029/2012GL051605.

Cramp, A., Vitaliano, C.J., Collins, M.B., 1989. Identification and dispersion of the Campanian ash layer (Y-5) in the sediments of the Eastern Mediterranean. Geo. Mar. Lett. 9, 19—25.

De Vivo., B., Rolandi, G., Gans., P.B., Calvert., A., Bohrson, W.A., Spera., F.J., Belkin., H.E., 2001. New constraints on the pyroclastic eruptive history of the Campanian volcanic Plain (Italy). Mineral. Petrol. 73, 47—65.

De Rijk, S., Hayes, A., Rohling., E.J., 1999. Eastern Mediterranean sapropel S1 interuption: and expression of the climatic deterioration around 7 ka BP. Mar. Geol. 153, 337—343.

Druitt, T.H., Mellors, R.A., Pyle, D.M., Sparks, R.S.J., 1989. Explosive volcanism on Santorini, Greece. Geol. Mag. 126, 95—126.

Druitt, T.H., Edwards, L., Mellors, R.M., Pyle, D.M., Sparks, R.S.J., Lanphere, M., Davies, M., Barriero, B., 1999. Santorini volcano. Geol. Soc. Mem. 19.

Druitt, T.H., Costa, F., Deloule, E., Scaillet, B., 2012. Decadal to monthly timescales of magma transfer and reservoir growth at a caldera volcano. Nature 482, 77—82.

Eastwood, W.J., Pearce, J.C., 1998. Recognition of Santorini (Minoan) tephra in lake sediments from Gölhisar Gölü, Southwest Turkey by Laser Ablation ICP-MS. J. Archaeol. Sci. 25, 677—687.

Eastwood, W.J., Pearce, N.J.G., Westgate, J.A., Perkins, W.T., Lamb, H.F., Roberts, N., 1999. Geochemistry of Santorini tephra in lake sediments from Southwest Turkey. Glob. Planet. Change 21, 17—19.

Federman, A.N., Carey, S.N., 1980. Electron microprobe correlation of tephra layers from Eastern Mediterranean. Quat. Res. 13, 160—171.

Giaccio, B., Nomade, S., Wulf, S., Isaia, R., Sottili, G., Cavuoto, G., Galli, P., Messina, P., Sposato, A., Sulpizio, R., Zanchetta, G., 2012. The late MIS 5 Mediterranean tephra markers: a reappraisal from peninsular. Quat. Sci. Rev. 56, 31—45.

Grant, K.M., Rohling, E.J., Bar-Matthews, M., Ayalon, A., Medina-Elizalde, M., Bronk Ramsey, C., Satow, C., Roberts, A.P., 2012. Rapid response of ice volume to polar temperature variations. Nature 491, 744—747.

Hamann, Y., Wulf, S., Ersoy, O., Ehrmann, W., Aydar, E., Schmiedl, G., 2010. First evidence of a distal early Holocene ash layer in Eastern Mediterranean deep-sea sediments derived from the Anatolian volcanic province. Quat. Res. 73, 497—506.

Hardiman, J., 1999. Deep sea tephra from Nisyros Island, Eastern Aegean Aea, Greece. Geol. Soc. Lond. Spec. Publ. 161, 69—88.

Hayes, A., Rohling, E.J., De Rijk, S., Kroon, D., Zacchariesse, W.J., 1999. Mediterranean planktonic foraminiferal faunas during the Last Glacial cycle. Mar. Geol. 153, 239—252.

Hunt, J.B., Hill, P.G., 1993. Tephra geochemistry: a discussion of some persistent analytical problems. Holocene 3, 271—278.

Iorio, M., Liddicoat, J., Budillon, F., Incoronato, A., Coa, R.S., Insinga, D.D., Cassata, W.S., Lubritto, C., Angelino, A., Tamburrino, S., 2014. Combined palaeomagnetic secular variation and petrophysical records to time-constrain geological and hazardous events: an example from the eastern Tyrrhenian Sea over the last 120 ka. Glob. Planet. Change 113, 91—109.

Jochum, K.P., Stoll, B., Herwig, K., Willbold, M., 2007. Validation of LA-ICP-MS trace element analysis of geological glasses using a new solid-state 193 nm Nd:YAG laser and matrix-matched calibration. J. At. Spectrom. 22, 112—121.

Keller, J., Ryan, W.B.F., Ninkovich, D., Altherr, R., 1978. Explosive volcanic activity in the Mediterranean over the past 20,000 year as recorded in deep sea sediments. Geol. Soc. Am. Bull. 89, 591—604.

Lane, C.S., Andric, M., Cullen, V., Blockley, S., 2011. The occurrence of distal Icelandic and Italian tephra in the Lateglacial of Lake Bled, Slovenia. Quat. Sci. Rev. 30, 1013—1018.

Le Bas, M.J., Le Maitre, R.W., Strckeisen, A., Zanettin, B., 1986. A chemical classification of volcanic rocks based on the total alkali-silica diagram. J. Petrol. 27, 745—750.

le Roux, P.J., le Roex, A.P., Schilling, J.-G., Shimizu, N., Perkins, W.W., Pearce, N.J.G., 2002. Mantle heterogeneity beneath the southern Mid-Atlantic Ridge: trace element evidence for contamination of ambient asthenospheric mantle. Earth Planet. Sci. Lett. 203, 479—498.

Lee, S., Bronk Ramsey, C., Hardiman, M., 2013. Modeling the age of the Cape Riva (Y-2) tephra. Radiocarbon 55, 741—747.

Lowe, J., Blockley, S., Trincardi, F., Asioli, A., Cattaneo, A., Matthews, I.P., Pollard, M., Wulf, S., 2007. Age modelling of late Quaternary marine sequences in the Adriatic: towards improved precision and accuracy using volcanic event stratigraphy. Cont. Shelf Res. 27, 560—582.

Lowe, J., Barton, N., Blockley, S., Bronk Ramsey, C., Cullen, V., Davies, W., Gamble, C., Grant, K., Hardiman, M., Housley, R., Lane, C., Lee, S., Lewis, M., MacLeod, A., Menzies, M., Muller, W., Pollard, M., Price, C., Roberts, A.P., Rohling, E.J., Satow, C., Smith, V.C., Stringer, C.B., Tomlinson, E.L., White, D., Albert, P., Arienzo, I., Barker, G., Boric, D., Carandente, A., Civetta, L., Ferrier, C., Guadelli, J.-L., Karkanas, P., Koumouzelis, M., Muller, U., Orsi, G., Pross, G., Rosi, M., Shalamanov-Korobar, L., Sirakov, N., Tzedakis, P.C., 2012. Volcanic ash layers illuminate the resilience of Neanderthals and early modern humans to natural hazards. Proc. Natl. Acad. Sci. 34, 13532—13537.

MacDonald, R., 1974. Nomenclature and petrochemistry of the peralkaline oversaturated extrusive rocks. Bull. Volcanol. 38, 489—516.

Margari, V., Pyle, D.M., Bryant, C., Gibbard, P.L., 2007. Mediterranean tephra stratigraphy revisited: results from a long terrestrial sequence on Lesvos Island, Greece. J. Volcanol. Geotherm. Res. 163, 34—54.

Marino, G., Rohling, E.J., Rijpstra, W.I.C., Sangiorgi, F., Schouten, S., Sininghe Damste, J.S., 2007. Aegean Sea as driver of hydrographic and ecological changes in the eastern Mediterranean. Geology 35, 675—678.

Marino, G., Rohling, E.J., Sangiori, F., Hayes, A., Casford, J.L., Lotter, A.F., Kucera, M., Brinkhuis, H., 2009. Early and middle Holocene in the Aegean Sea: interplay between high and low latitude climate variability. Quat. Sci. Rev. 28, 3246—3262.

Müller, W., Shelley, M., Miller, P., Broude, S., 2009. Initial performance metrics of a new custom-designed ArF eximer LA-ICPMS system coupled to a two-volume laser-ablation cell. J. Anal. At. Spectrom. 24, 209—214.

Narcisi, B., Vezzoli, L., 1999. Quaternary stratigraphy of distal tephra layers in the Mediterranean—an overview. Glob. Planet. Change 21, 31—50.

Osbourne, A.H., Marino, G., Vance, D., Rohling, E.J., 2010. Eastern Mediterranean surface water Nd during Eemian sapropel S5: monitoring northerly (mid-latitude) versus southerly (sub-tropical) freshwater contributions. Quat. Sci. Rev. 29, 2473—2483.

Paterne, M., Guichard, F., Duplessy, J.C., Siani, G., Sulpizio, R., Labeyrie, J., 2008. A 90,000—200,000 yrs marine tephra record of Italian volcanic activity in the central Mediterranean and Sea. J. or Volcanol. Geotherm. Res. 177, 187—196.

Pearce, N.J.G., Bendall, C.A., Westgate, J.A., 2008. Comment on "Some numerical considerations in the geochemical analysis of distal crypto-tephra" by A.M. Pollard, S.P.E.Blockley and C.S.Lane. Appl. Geochem. 23, 1353—1364.

Pearce, N.J.G., Westgate, J.A., Perkins, W.T., Preece, S.J., 2004. The application of ICP-MS methods to tephrochronological problems. Appl. Geochem. 19, 289—322.

Pyle, M.D., Rickets, G.D., Margari, V., van Andel, T.H., Sinitsyn, A.A., Praslov, N., Lisitsyn, S., 2006. Wide dispersal and dposition of distal tephra during the Pleistocene Campanian Ignimbrite/Y5 eruption, Italy. Quat. Sci. Rev. 25, 2713—2728.

Richardson, D., Ninkovich, D., 1976. Use of K_2O, Rb, Zr, and Y versus SiO_2 in volcanic ash layers of the eastern Mediterranean to trace their source. Bull. Geol. Soc. Am. 87, 110—116.

Rohling, E.J., Cane, T.R., Cooke, S., Sprovieri, M., Bouloubassi, I., Emeis, K.C., Schiebel, R., Kroon, D., Jorissen, F.J., Lorre, A., Kemp, A.E.S., 2002a. African monsoon variability during the previous interglacial maximum. Earth Planet. Sci. Lett. 202, 61—75.

Rohling, E.J., Mayewski, P.A., Abu-Zied, R.H., Casford, J.S.L., Hayes, A., 2002b. Holocene atmosphere-ocean interations: records from Greenland and the Aegean Sea. Clim. Dyn. 18, 587—593.

Rohling, E.J., Sprovieri, M., Cane, T., Casford, J.S.L., Cooke, S., Bouloubassi, I., Emeis, K.C., Schiebel, R., Rogerson, M., Hayes, A., Jorissen, F.J., Kroon, D., 2004. Reconstructing past planktic foraminiferal habitats using stable isotope data: a case history for Mediterranean sapropel S5. Mar. Micropaleontol. 50, 89—123.

Schiano, P., Clocchiatti, R., Ottolini, L., Busa', I., 2001. Transition of Mount Etna lavas from a mantle-plume to an island-arc magmatic source. Nature 412, 900—904.

Schiano, P., Clocchiatti, R., Ottolini, L., Sbrana, A., 2004. The relationship between potassic, calc-alkaline and Na-alkaline magmatism in South Italy volcanoes: a melt inclusion approach. Earth Planet. Sci. Lett. 220, 121—137.

Siani, G., Sulpizio, R., Paterne, M., Sbrana, A., 2003. Tephrostratigraphy study for the last 18,000 ^{14}C years in a deep-sea sediment sequence for the South Adriatic. Quat. Sci. Rev. 23, 2485—2500.

Smith, P.E., York, D., Chen, Y., Evensen, N.M., 1996. Single crystal $^{40}Ar—^{39}Ar$ dating of a Late Quaternary paroxysm on Kos, Greece: concordance of terrestrial and marine ages. Geophys. Res. Lett. 23, 3047—3050.

Smith, P.E., Evensen, N.M., York, D., 2000. Under the volcano; a new dimension in Ar—Ar dating of volcanic ash. Geophys. Res. Lett. 27 (5), 585—588.

Smith, V.C., Isaia, R., Pearce, N.J.G., 2011. Tephrostratigraphy and glass compositions of post-15 kyr Campi Flegrei eruptions: implications for eruption history and

chronostratigraphic markers. Quat. Sci. Rev. 30, 3638—3660. http://dx.doi.org/10.1016/j.quascirev.2011.07.012.

Sparks, R.S.J., Brazier, S., Huang, T.C., Muerdter, D., 1983. Sedimentology of the Minoan deep-sea tephra layer in the Aegean and Eastern Mediterranean. Mar. Geol. 54, 131—167.

St Seymour, K., Christianis, K., 1995. Correlation of a tephra layer in Western Greece with a late Pleistocene eruption in the Campanian province of Italy. Quat. Res. 43, 46—54.

St Seymour, K., Christanis, K., Bouzinos, A., Papazisimou, S., Papatheodorou, G., Moran, E., Denes, G., 2004. Tephrostratigraphy and tephrochronology in the Philippi peat basin, Macedonia, Northern Hellas (Greece). Quat. Int. 121, 53—65.

Tamburrino, S., Insignia, D.D., Sprovieri, M., Petrosino, P., Tiepolo, M., 2012. Major and trace element characterisation of tephra layers offshore Pantelleria Island: insights into the last 200 ka of volcanic activity and the contribution to the Mediterranean tephrochronology. J. Quat. Sci. 27, 129—140.

Tomlinson, E.L., Thordarson, T., Muller, W., Thirlwall, M., Menzies, M.A., 2010. Microanalysis of tephra by LA-ICP-MS-Strategies, advantages and limitations assessed using the Thorsmork ignimbrite (Southern Iceland). Chem. Geol. 279, 73—89.

Tomlinson, E.L., Arenzo, I., Civetta, L., Wulf, S., Smith, V.C., Hardiman, M., Lane, C.S., Carandente, A., Orsi, G., Rosi, M., Muller, W., Menzies, M.A., 2012. Geochemistry of the Phlegrean Fields (Italy) proximal sources for major Mediterranean tephra: implications for the dispersal of Plinian and co-ignimbritic components of explosive eruptions. Geochim. Cosmochim. Acta 93, 102—128.

Tomlinson, E.L., Smith, V.C., Albert, P.G., Aydar, E., Civetta, L., Cioni, R., Çubukçu, E., Gertisser, R., Isaia, R., Menzies, M.A., Orsi, G., Rosi, M., Zanchetta, G., 2014. The major and trace element glass compositions of the productive Mediterranean volcanic sources: tools for correlating distal tephra layers in and around Europe. Quat. Sci. Rev. http://dx.doi.org/10.1016/j.quascirev.2014.10.028.

Van de Meer, M.T.J., Baas, M., Rijpstra, W.I.C., Marine, G., Rohling, E.J., Sinninghe Damste, J.S., Schouten, S., 2007. Hydrogen isotopic compositions of long-chain alkenones record freshwater flooding of the Eastern Mediterranean and the onset of sapropel deposition. Earth Planet. Sci. Lett. 262, 594—600.

Vezzoli, L., 1991. Tephra layers in Bannock Basin (Eastern Mediterranean). Mar. Geol. 100, 21—34.

Vespa, M., Keller, J., Gertisser, R., 2006. Interplinian explosive activity of Santorini volcano (Greece) during the past 150,000 years. J. Volcanol. Geotherm. Res. 153, 262—286.

Vinci, A., 1984. Chemical differences between the island and submarine pumice layers of Thera. Mar. Geol. 55, 487—491.

Vinci, A., 1985. Distribution and chemical composition of tephra layers from the Eastern Mediterranean abyssal sediments. Mar. Geol. 64, 143—155.

Vitaliano, C.J., Taylor, S.R., Farrand, W.R., Jacobsen, T.W., 1981. Tephra layer in Franchthi Cave, Peleponnesos, Greece. Tephra Stud. NATO Adv. Study Inst. Ser. 75, 373—379.

Vogel, H., Zanchetta, G., Sulpizio, R., Wagner, B., Nowaczyk, N., 2010. A tephrostratigraphic record for the Last Glacial-Interglacial cycle from Lake Ohrid, Albania and Macedonia. J. Quat. Sci. 25, 320—338.

Watkins, N.D., Sparks, R.S.J., Sigurdsson, H., Huang, T.C., Federman, A., Carey, S., Ninkovich, D., 1978. Volume and extent of the Minoan tephra from the Santorini volcano: new evidence from deep sea cores. Nature 271, 122—126.

WoldeGabriel, G., Hart, W.K., Heiken, G., 2005. Innovative tephra studies in the East African rift system. Trans. Am. Geophys. Union 86, 255—256.

Wulf, S., Kraml, M., Kuhn, T., Schwarz, M., Inthorn, M., Keller, J., Kuscu, I., Halback, P., 2002. Marine tephra from the Cape Riva Eruption (22 ka) of Santorini in the Sea of Marmara. Mar. Geol. 183, p131—141.

Wulf, S., Kraml, M., Brauer, A., Keller, J., Negendank, J.F.W., 2004. Tephrochronology of the 100 ka lacustrine sediment record of Lago Grande di Monticchio (southern Italy). Quat. Int. 122, 7—30.

Wulf, S., Keller, J., Paterne, M., Mingram, J., Lauterbach, S., Opitz, S., Sottili, G., Giaccio, B., Albert, P.G., Satow, C., Tomlinson, E., Viccaro, M., Brauer, A., 2012. The 100—133 ka record of Italian explosive volcanism and revised tephrochronology of Lago Grande di Monticchio. Quat. Sci. Rev. 58, 104—123.

Zanchetta, G., Sulpizio, R., Roberts, N., Cioni, R., Eastwood, W.J., Siani, G., Caron, B., Paterne, M., Santacroce, R., 2011. Tephrostratigraphy, chronology and climatic events of the Mediterranean basin during the Holocene: an overview. Holocene 21, 33—52.